THE PHOTOCHEMISTRY OF μ-PYRAZINEDECAAMMINERHODIUM(III)RUTHENIUM(II) PERCHLORATE AND μ-(4-CYANO-*ΩN*(Ru)-PYRIDINE-*ΩN*(Rh))-DECAAMMINERHODIUM(III)RUTHENIUM(II) PERCHLORATE

by

JANETTE ANN GELROTH

B.A., Bethany College, 1975

A MASTER'S THESIS

submitted in partial fulfillment of the

requirements for the degree

MASTER OF SCIENCE

Department of Chemistry

KANSAS STATE UNIVERSITY
Manhattan, Kansas

1979

Approved by:

Major Professor

Document
LD
266T
.T4
1979
G44
c.2

Table of Contents

Abbreviations . . . iii

List of Figures . . . iv

List of Tables . . . v

Acknowledgements . . . vi

Introduction . . . 1

- A. Photochemistry . . . 2
- B. Electronic Transitions . . . 4
- C. Excited State Classifications . . . 6
- D. Photochemical Processes of Rh(III) Ammines . . . 9
- E. Photochemical Processes of Ru(II) Ammines . . . 13
- F. Binuclear Complexes . . . 17
- G. Nomenclature . . . 19
- H. Statement of the Problem . . . 21

Experimental . . . 23

- A. Materials . . . 24
- B. Syntheses . . . 24
  - 1. Chloropentaamminerhodium(III) chloride, $[Rh(NH_3)_5Cl]Cl_2$ . . . 24
  - 2. Aquopentaamminerhodium(III) perchlorate, $[Rh(NH_3)_5H_2O][ClO_4]_3$ . . . 25
  - 3. Pentaamminepyrazinerhodium(III) perchlorate, $[Rh(NH_3)_5pyz][ClO_4]_3$ . . . 25
  - 4. Chloropentaammineruthenium(III) chloride, $[Ru(NH_3)_5Cl]Cl_2$ . . . 26
  - 5. μ-Pyrazinedecaamminerhodium(III)ruthenium(II) perchlorate, $[(NH_3)_5Rh(pyz)Ru(NH_3)_5][ClO_4]_5$ . . . 26
  - 6. (4-cyanopyridine-ΩN)pentaamminerhodium(III) perchlorate, $[Rh(NH_3)_5pyCN][ClO_4]_3$ . . . 28
  - 7. (4-cyano-ΩN-pyridine)pentaammineruthenium(II) perchlorate, $[Ru(NH_3)_5NCpy][ClO_4]_2$ . . . 29
  - 8. μ-(4-cyano-ΩN(Ru)-pyridine-ΩN(Rh))decaammine-rhodium(III)ruthenium(II) perchlorate, $[(NH_3)_5Rh(pyCN)Ru(NH_3)_5][ClO_4]_5$ . . . 30
  - 9. 4-cyanopyridinium trifluoroacetate, $4\text{-}NCpyH^+\text{-}CF_3CO_2^-$ . . . 31
  - 10. Azidopentaamminerhodium(III) perchlorate, $[Rh(NH_3)_5N_3][ClO_4]_2$ . . . 31
  - 11. (4-cyano-ΩN-pyridine)pentaamminerhodium(III) perchlorate, $[Rh(NH_3)_5NCpy][ClO_4]_3$
    - a. From aquopentaamminerhodium(III) perchlorate . . . 32
    - b. From azidopentaamminerhodium(III) perchlorate . . . 33

    12. μ-(4-cyano-Ω*N*(Rh)-pyridine-Ω*N*(Ru))decaammine-rhodium(III)ruthenium(II) perchlorate, $[(NH_3)_5Rh(NCpy)Ru(NH_3)_5][ClO_4]_5$ 33
    13. (4-cyanopyridine-Ω*N*)pentaammineruthenium(II) perchlorate, $[Ru(NH_3)_5pyCN][ClO_4]_2$ 34
  C. Analyses 35
  D. Spectra 35
  E. Photolysis Apparatus and Procedures 36
  F. Carbon-13 NMR Spectra 40

Results 41

  A. Spectral Characteristics 42
    1. Electronic spectra 42
    2. Infrared spectra 44
    3. Carbon-13 nuclear magnetic resonance spectra 44
  B. Photolyses 47
    1. $[Rh(NH_3)_5pyz][ClO_4]_3$ 47
    2. $[(NH_3)_5Rh(pyz)Ru(NH_3)_5][ClO_4]_5$ 49
    3. $[Rh(NH_3)_5pyCN][ClO_4]_3$ 49
    4. $[Ru(NH_3)_5NCpy][ClO_4]_2$ 50
    5. $[(NH_3)_5Rh(pyCN)Ru(NH_3)_5][ClO_4]_5$ 50

Discussion 53

  A. 4-Cyanopyridine Complexes of $Fe(CN)_5^{3-}$, $Ru(NH_3)_5^{2+}$, $Co(CN)_5^{2-}$, and $Rh(NH_3)_5^{3+}$ 54
  B. Photolyses 56

Conclusion 68

References 71

Appendix A (Quantum Yield Calculation) 76

Appendix B (Photolysis Data) 82

Abstract

Abbreviations

acn: acetonitrile

bipy: 2,2'-bipyridine

bzn: benzonitrile

en: ethylenediamine

phen: 1,10-phenanthroline

py: pyridine

ic: internal conversion

isc: intersystem crossing

IL: internal ligand

LF: ligand field

LMCT: ligand-to-metal charge transfer

MLCT: metal-to-ligand charge transfer

List of Figures

Figure 1 Molecular orbital diagram (O_h symmetry) illustrating possible electronic transitions 7

Figure 2 Energy level diagram illustrating internal conversion/intersystem crossing from a directly irradiated excited state to a lower energy excited state 10

Figure 3 Excited-state diagrams illustrating the proposed mechanism for the photoreaction of $Ru(NH_3)_5py\text{-}X^{2+}$ 16

Figure 4 Schematic diagram of apparatus used in the syntheses of binuclear complexes 27

Figure 5 Schematic diagram of optical train apparatus 37

Figure 6 Schematic diagram of deoxygenation apparatus 38

Figure 7 Potential energy curve illustrating excitation of a ground state molecule 60

Figure 8 Energy level diagram for $(NH_3)_5Ru(NCpy)Rh(NH_3)_5{}^{5+}$ 62

Figure 9 Energy level diagram for $(NH_3)_5Ru(pyz)Rh(NH_3)_5{}^{5+}$ 65

List of Tables

Table I	Photochemical and Photophysical Properties of $Rh(NH_3)_5L^{3+}$ Complexes	12
Table II	Spectroscopic Quantum Yields for the Photoaquation of $Ru(NH_3)_5L^{2+}$ in Aqueous Solution	15
Table III	Electronic Absorption Spectra of Various Rhodium and Ruthenium Ammine Complexes	43
Table IV	Nitrile Stretching Frequencies of Various Rhodium and Ruthenium Ammine Complexes	5
Table V	^{13}C Nuclear Magnetic Resonance Chemical Shifts of $[Rh(NH_3)_5pyCN][ClO_4]_3$ and 4-Cyanopyridine, Free Ligand	46
Table VI	Irradiation Wavelengths and Quantum Yields for the Complexes Photolyzed	48

Acknowledgements

I wish to express my gratitude to Dr. John Petersen for his guidance and encouragement in the completion of this project. Also, thanks are due to Dr. Keith Purcell and Dr. Kenneth Kay for their helpful comments and advice on this manuscript. Appreciation is expressed to all the others, especially Joe Figard, Dave Wohlers, Frank Jakse, and Kurt Van Tassel, who have helped me through their friendship and encouragement. I also wish to express a special thanks to my husband, Joe, for his patience and understanding.

INTRODUCTION

A. Photochemistry

Photochemistry is a field associated with the physical and chemical consequences of electronic excitation, which occurs when light and matter interact. Two laws which govern photochemical reactions are: 1) "only radiations which are absorbed by the reacting system can be effective in producing chemical changes" (Grotthus, 1877; Draper, 1841)[1], and 2) "each light quantum absorbed activates one molecule" (with the exception of biphotonic processes which occur as a result of high intensity irradiation) (Stark, 1908-12; Einstein, 1912-13)[1]. Thus, the absorbed light causes electronic excitation of a molecule, and it is from this excited molecule, or a subsequent intermediate, that all the photochemical processes occur.

The primary processes which can occur as a result of photon absorption are summarized in equations (1)-(4).

$A + h\nu \longrightarrow A^*$	absorption	(1)
$A^* \xrightarrow{k_1} A + \text{heat}$	nonradiative deactivation	(2)
$A^* \xrightarrow{k_2} A + h\nu'$	radiative deactivation	(3)
$A^* \xrightarrow{k_3} \text{products}$	photochemical reaction	(4)

The efficiency of a particular process is given by the quantum yield (Φ), which is defined as:

$$\Phi_a = \frac{\#\text{ molecules undergoing process a}}{\#\text{ photons absorbed}}$$

or

$$\Phi_a = \frac{dP/dt}{I_a}$$

where dP/dt is the rate of formation of a, and I_a is the intensity absorbed by the system. A general conclusion concerning the quantum yield for product formation has been developed using a steady state approximation. From equations (1)-(4), the rate of formation of the product is:

$$dP/dt = k_3\ [A^*] \tag{5}$$

Application of the steady state approximation to [A*] gives:

$$\frac{d[A^*]}{dt} = 0 = I_a - k_1\ [A^*] - k_2\ [A^*] - k_3\ [A^*] \tag{6}$$

or

$$[A^*] = \frac{I_a}{k_1 + k_2 + k_3} \tag{7}$$

Substitution into equation (5) yields:

$$\frac{dP}{dt} = \frac{k_3 I_a}{k_1 + k_2 + k_3} \tag{8}$$

Using the above definition of a quantum yield, it is determined that

$$\Phi = \frac{k_3}{k_1 + k_2 + k_3} \tag{9}$$

Equation (9) applies to systems in which A* is populated directly by irradiation. For systems in which the excited state is indirectly populated by intersystem crossing/internal conversion, the efficiency of this indirect population (Φ_{isc}) must also be incorporated, as in equation (10).

$$\Phi = \Phi_{isc} \frac{k_3}{k_1 + k_2 + k_3} \tag{10}$$

The summation of the quantum yields for all the primary processes in a given system should equal 1.[2]

B. Electronic Transitions

Two criteria must be met in order for a molecule to absorb light. First, the energy of the light must match the difference in ground and excited state energies of the molecule (equation 11), where E_{gs} is the

$$h\nu = E_{es} - E_{gs} \tag{11}$$

energy of the ground state with wave function Ψ_{gs}, and E_{es} is the energy of the excited state with wave function Ψ_{es}. Second, an interaction must generally occur between the electric or magnetic vector components of the radiation and the electric or magnetic dipoles of the molecule (the electric interactions are the major contributor to transitions).[3]

If these two criteria are satisfied, the probability of a transition occurring can be determined from the transition-moment integral R (equation 12), where $\hat{d}$ is the dipole moment operator. This operator

$$R = \langle \Psi_{es} | \hat{d} | \Psi_{gs} \rangle \tag{12}$$

can be separated into a sum over electrons and a sum over nuclei (equation 13). The molecular wave function Ψ can be factored (approximately)

$$\hat{d} = \hat{d}_{el} + \hat{d}_{N} \tag{13}$$

into electronic and nuclear eigenfunctions (equation 14). Incorpora-

$$\Psi = \psi_{el}\, \psi_{N} \tag{14}$$

tion of equations (13) and (14) into equation (12) gives

$$\begin{aligned}\langle \Psi_{es}|\hat{d}|\Psi_{gs}\rangle &= \iint \psi^*_{es,el}\psi^*_{es,N}(\hat{d}_{el} + \hat{d}_N)\psi_{gs,el}\psi_{gs,N}d\tau_{el}d\tau_N \\ &= \int\psi^*_{es,N}\psi_{gs,N}[\int\psi^*_{es,el}\hat{d}_{el}\psi_{gs,el}d\tau_{el}]d\tau_N \\ &\quad + \int\psi^*_{es,N}\hat{d}_N\psi_{gs,N}[\int\psi^*_{es,el}\psi_{gs,el}d\tau_{el}]d\tau_N \qquad (15)\end{aligned}$$

Since $\psi_{es,el}$ and $\psi_{gs,el}$ are eigenfunctions of the Hermitian operator $\hat{H}_{el}$ with different eigenvalues, they are orthogonal. Equation (15) can, therefore, be reduced to

$$\langle \Psi_{es}|\hat{d}|\Psi_{gs}\rangle = \int\psi^*_{es,N}\psi_{gs,N}[\int\psi^*_{es,el}\hat{d}_{el}\psi_{gs,el}d\tau_{el}]d\tau_N \qquad (16)$$

In order for a transition to be forbidden, equation (16) must equal zero. Two principal selection rules have been developed which pertain to vanishing of the bracketed portion of equation (16). When spin-orbit interaction is small, $\psi_{es,el}$ and $\psi_{gs,el}$ are eigenfunctions of the Hermitian operator $\hat{S}^2$ (the square of the magnitude of the total spin angular momentum of a particle). Since $\hat{S}^2$ commutes with $\hat{d}_{el}$, electronic transitions with a change in S are forbidden.[2] In heavy atom systems, where spin-orbit coupling is strong, this spin selection rule breaks down, allowing transitions with typical ε values of ~1 to 10 $M^{-1}cm^{-1}$ to occur between states of different multiplicity.

The second selection rule deals with parity. The product $\psi_{es,el}\hat{d}_{el}\psi_{gs,el}$ must be totally symmetric under the extant group operations for its integral to be non-zero. When the inversion symmetry element is present, the components of $\hat{d}$ are ungerade, and $\psi_{es,el}\hat{d}_{el}$-$\psi_{gs,el}$ must be gerade to have a non-zero integral. Therefore, it is necessary for $\psi_{es,el}$ and $\psi_{gs,el}$ to be of unequal parity. This is the basis of the Laporte-forbidden or parity-forbidden selection rule, which states that transitions between orbitals of the same parity (i.e., g → g, or u → u) are forbidden in centro-symmetry. Coupling between the vibrational and electronic functions assists in the breakdown of the Laporte selection rule, and transitions of this type can occur and typically have ε values in the range of ~10 to 100 $M^{-1}cm^{-1}$.

C. Excited State Classifications

Although the extent of metal and ligand orbital mixing varies, it is most convenient to categorize electronic transitions by assuming that the original metal ion electrons remain localized mainly on the metal and that the original ligand electrons are localized mainly on the ligand. Based on this simplification, electronic transitions can be classified as follows: 1) ligand field (metal localized), LF, 2) internal ligand (ligand localized), IL, and 3) charge transfer (a) ligand-to-metal, LMCT, (b) metal-to-ligand, MLCT, and (c) metal-to-solvent, MSCT. (The metal-to-solvent charge transfer transition is difficult to treat theoretically. Since it does not pertain to the work described here, it will not be discussed.) Figure 1 is a simplified molecular orbital diagram illustrating these possible transitions.

Equations (17)-(21) describe a conceptualized view of the various transitions and their resulting excited states for a d^6 system of O_h symmetry.[4]

$$[M^{r+}(t_{2g}{}^{6})L_6]^{n+} \xrightarrow[LF]{h\nu} [M^{r+}(t_{2g}{}^{5}e_g{}^{1})L_6]^{n+\,*} \tag{17}$$

$$[M^{r+}L_5L(\pi_m)]^{n+} \xrightarrow[IL]{h\nu} [M^{r+}L_5L(\pi_{m-1}\pi^*)]^{n+\,*} \tag{18}$$

$$[M^{r+}L_6]^{n+} \xrightarrow[LMCT]{h\nu} [M^{(r-1)+}(L_6{}^{+})]^{n+\,*} \tag{19}$$

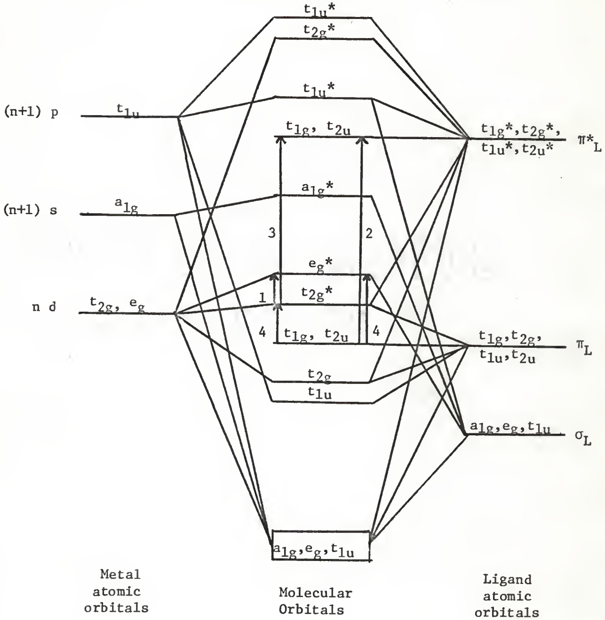

1) Ligand Field (LF)

2) Internal Ligand (IL)

3) Metal-to-Ligand Charge Transfer (MLCT)

4) Ligand-to-Metal Charge Transfer (LMCT)

Figure 1. Molecular orbital diagram (O_h symmetry) illustrating possible electronic transitions.

$$[M^{r+}L_6]^{n+} \xrightarrow[\text{MLCT}]{h\nu} [M^{(r+1)+}(L_6^{-})]^{n+\,*} \tag{20}$$

$$[M^{r+}L_6]^{n+} \xrightarrow[\text{MSCT}]{h\nu} [M^{(r+1)+}L_6]^{(n+1)+} + e^{-} \tag{21}$$

Ligand field excitation results in the motion of an electron between two d orbitals primarily localized on the metal. For a d^6 system, this transition results in an angular redistribution of the charge from a t_{2g} orbital, which is directed between the ligands, to an e_g^* orbital, which is directed toward the ligands. The increased antibonding character between the metal and ligands in populating e_g^* presumably leads to lengthening of the metal-ligand bonds for the excited state structure and may result in loss of a ligand. Thus, photosubstitution (as given in equation 22) of the complex might be

$$ML_n + X \xrightarrow{h\nu} ML_{n-1}X + L \tag{22}$$

expected to occur as a result of LF irradiation.

Similarly, excitation into a charge transfer excited state results in a radial redistribution of the electronic charge, where the electron can be envisioned as migrating from a molecular orbital which is localized mainly on the metal to one which is localized mainly on the ligand, or vice versa. Depending upon various considerations, such as the effective amount of charge being transferred and environmental effects (solvent reactivity, pH, cage effects)[1], a charge transfer excited state might potentially lead to an intramolecular oxidation-reduction reaction.

These generalizations, concerning types of reactions which should follow formation of a particular excited state, are easily made but cannot be considered rigorous. The excited state formed directly by absorption may undergo radiative deactivation before a reaction can occur, or nonradiative deactivation to indirectly populate states lower in energy by internal conversion/intersystem crossing from the initially populated state (as illustrated in Figure 2). Thus, the reaction observed may be considerably different from that expected from formation of a particular excited state.

D. Photochemical Processes of Rh(III) Ammines

Photochemical and photophysical studies have been reported on various rhodium(III)-ammine complexes. Included among these are $Rh(NH_3)_5X^{2+}$ (X = halogen)[5,6], $RhA_4X_2^+$ (A_4 = $(NH_3)_4$, $(py)_4$, $(en)_2$, $(bipy)_2$, or $(phen)_2$; X = Cl, Br, or I)[7], and $Rh(NH_3)_5L^{3+}$ (L = a neutral nitrogen coordinating base)[8,9,10]. Unlike its first row homolog Co(III)[1,5,6], Rh(III) complexes have been shown to be photochemically more reactive upon ligand field excitation (quantum yield values range from ~2 x 10^{-4} to 0.1 for certain $Co(NH_3)_5L^{3+}$ complexes and from 0.02 to 0.9 for analogous $Rh(NH_3)_5L^{3+}$ complexes.

The halopentaamminerhodium(III) complexes undergo photoaquation in aqueous solution when the LF bands are irradiated. The ligand which is labilized, however, depends upon which halogen is present in the complex. For X = Cl, the chloride is replaced as in equation (23),

$$Rh(NH_3)_5Cl^{2+} \xrightarrow[H_2O]{h\nu} Rh(NH_3)_5OH_2^{3+} + Cl^- \qquad (23)$$

and for X = I, irradiation results in labilization of an ammine ligand (equation 24). When the halogen is Br, both NH_3 and Br^- can be labil-

$$Rh(NH_3)_5I^{2+} \xrightarrow[H_2O]{h\nu} \underline{trans}\text{-}Rh(NH_3)_4OH_2I^{2+} \qquad (24)$$

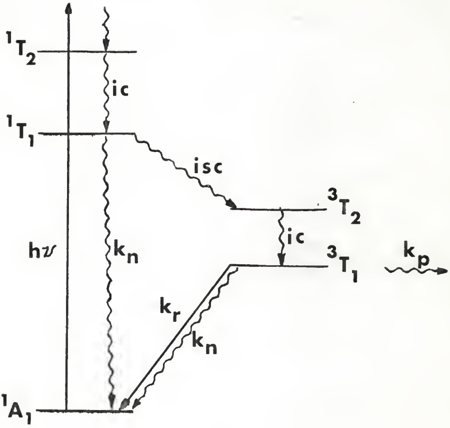

Figure 2. Energy level diagram (d^6, O_h) illustrating internal conversion/intersystem crossing from a directly irradiated excited state to a lower energy excited state. i.c., internal comversion; i.s.c., intersystem crossing; k_p, photoreaction; k_n and k_r, nonradiative and radiative deactivation, respectively.

ized. The photoreaction in equation (23) has also been found to occur indirectly as a result of photosensitization.[5] Irradiation of biacetyl solutions containing effectively non-absorbing quantities of $Rh(NH_3)_5Cl^{2+}$ leads to formation of $Rh(NH_3)_5OH_2^{3+}$ and quenching of the biacetyl phosphorescence. From varying the concentration of the quencher, Kelly and Endicott have concluded that the photochemical reaction in equation (23) occurs from the triplet LF state and that the intersystem crossing quantum yield is near unity.

Ligand field photolyses of $RhA_4X_2^+$ (A_4 = $(NH_3)_4$, $(py)_4$, $(en)_2$, $(bipy)_2$, or $(phen)_2$; X = Cl, Br, or I) in aqueous solution led to photoaquation of the halide. In addition, when A_4 = $(en)_2$[7] or $(NH_3)_4$[11], and X = Cl, it has been observed that photoaquation of the cis isomers can be accompanied by isomerization to form the trans products. Photosubstitution reactions of the trans compounds led to stereoretentive products.

The ligand field irradiation of $Rh(NH_3)_5L^{3+}$, where L is NH_3, py, bzn, or acn, results in photoaquation of the unique ligand, L, as the major photoreactive pathway.[9,10] Table I summarizes the photochemical and photophysical data for various $Rh(NH_3)_5L^{3+}$ complexes. The absorbance maxima of the various $Rh(NH_3)_5L^{3+}$ complexes are not greatly affected by changing the unique ligand L or substituents on L. The quantum yields, however, are somewhat affected, with the Φ_L values varying approximately inverse to the basicity of the ligand. E_T, the energy of the emitting state (presumed to be the $^3E^a$ state) is calculated from emission data[9] (equation 25), and tends to decrease with

$$E_T = \nu_{max} + 1.29\Delta\nu_{\frac{1}{2}} \qquad (25)$$

Table I. Photochemical and Photophysical Properties of $Rh(NH_3)_5L^{3+}$ Complexes.[a]

L	λ_{max} (nm)	$pK_a(L)$[b]	Φ_L[c] (moles/ein.)	E_T[d] (kK)
NH_3	305	9.3	0.075	21.2
4-Mepy	302	6.0	0.091	21.4
py	302	5.3	0.14	21.0
3-Clpy	302	2.8	0.34	20.0
bzn	300	~-10	0.35	21.2
acn	301	~-10	0.47	20.3

[a] Reference 9

[b] pK_a of free ligand

[c] λ_{irr} = 313 nm, dilute aqueous solution

[d] At 77° K in $MeOH/H_2O$ (4/1, v/v) glass

decreasing ligand basicity. Thus, for $Rh(NH_3)_5L^{3+}$ complexes, the unique ligand L, or variations in substituents on L, affects to a minor extent the quantum yield values and the energy of the emitting state. In all cases observed, however, the primary photoreactive pathway was aquation of L.

E. Photochemical Processes of Ruthenium(II) Ammines

The absorption spectrum of $Ru(NH_3)_5py^{2+}$ is dominated by an internal ligand $\pi^* \leftarrow \pi$ band at 244 nm ($\varepsilon_{max} = 4.56 \times 10^3\ M^{-1}cm^{-1}$) and a MLCT band at 407 nm ($\varepsilon_{max} = 7.78 \times 10^3\ M^{-1}cm^{-1}$).[12] Irradiation of the MLCT band of this complex results almost exclusively in photosubstitution reactions (equation 26).[8,12,13]

$$Ru(NH_3)_5py^{2+} + H_2O \xrightarrow{h\nu} \begin{cases} Ru(NH_3)_5OH_2^{2+} + py \\ \underline{cis}\text{- and } \underline{trans}\text{-}Ru(NH_3)_4\text{-} \\ \qquad H_2Opy^{2+} + NH_3 \end{cases} \tag{26}$$

The cis and trans aquopyridine-Ru(II) products in equation (26) have MLCT bands similar in wavelength and intensity to that of the starting material (cis, 400 nm, $\varepsilon = 6.6 \times 10^3\ M^{-1}cm^{-1}$; trans, 403 nm, $\varepsilon = 7.8 \times 10^3\ M^{-1}cm^{-1}$).[12] Therefore, a quantum yield calculation based on the spectrochemical disappearance of the MLCT band would approximate the photoaquation of pyridine to form $Ru(NH_3)_5OH_2^{2+}$ (which is essentially transparent in the visible region).

The excited state MLCT*, resulting from charge transfer excitation,

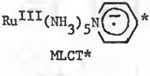

MLCT*

can be conceptualized as the oxidized metal ion bound to a radical anion pyridine ligand. Ru(III) amine complexes are characteristically inert to substitution reactions[14], so it is presumed that MLCT* would not inherently lead to photosubstitution reactions. Thus, it has been proposed[8,13] that a ligand field state, lower in energy than the charge transfer state, is responsible for the photoaquation of the pyridine.

Changes in L or in substituents on L have dramatic effects on the MLCT band maxima of $Ru(NH_3)_5L^{2+}$, with the more electron-withdrawing groups red-shifting the band, and electron-donating groups resulting in blue-shifts.[8] It is assumed that variation of the substituent on L does not substantially affect the energies of the LF bands, similar to observations made on the Rh(III) complexes.[10] Ford and coworkers[8,13] have prepared and photolyzed various $Ru(NH_3)_5L^{2+}$ complexes in an effort to "tune" the MLCT excited state to be above or below the LF excited state. Table II summarizes their data. Those complexes with λ_{max}(MLCT) $\leq$ 460 nm have quantum yield values of 0.02 - 0.05 moles/ein. for the photoaquation of L, and have been termed "reactive". In these complexes, the $^3E^a$ ($^3T_1$ in O_h) state is proposed to lie at an energy lower than that of the ^{3}CT, and thus the photoreaction occurs out of the lowest, or E^a, excited state. The "unreactive" complexes, those with $\lambda_{max} \geq$ 490 nm and Φ_{py-X} values less than 3×10^{-4} moles/ein., have the relatively nonlabile ^{3}CT as the lowest energy excited state. Figure 3 shows simplified excited-state diagrams representing the proposed mechanisms for the reactive and unreactive cases. (These diagrams differ in energy level positioning from the mechanism proposed as a result of this research. This mechanism will be presented and discussed in the Discussion section.)

Table II. Spectroscopic Quantum Yields for the Photoaquation of $Ru(NH_3)_5L^{2+}$ in Aqueous Solution.[a]

L	$\lambda_{max}(CT)^b$	λ_{irr}^b	Φ_L^c
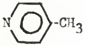	398	405	37 ± 3
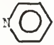	408	405	45 ± 2
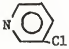	426	436	48 ± 2
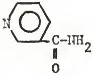	427	433	8.5 ± 0.2
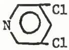	447	450	42 ± 2
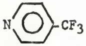	454	455	22 ± 5
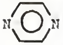	472	475	1.4 ± 0.1
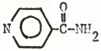	479	480	1.07 ± 0.04
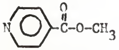	495	500	0.28 ± 0.04
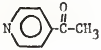	523	520	0.25 ± 0.06
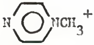	540	540	0.04 ± 0.01
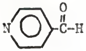	545	546	0.05 ± 0.01

[a] Reference 8

[b] in nm

[c] in moles/ein. (x 10^3)

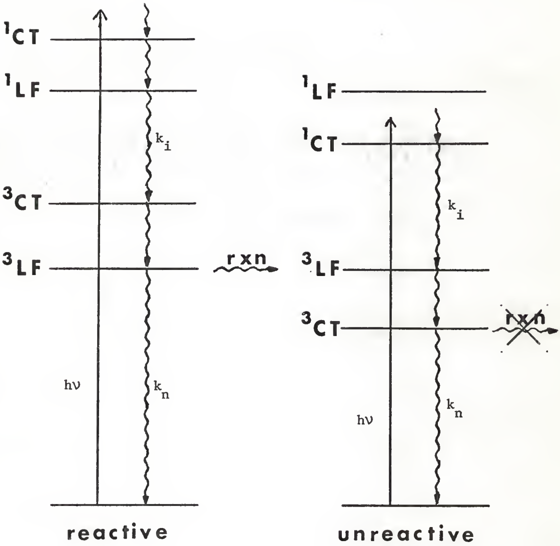

Figure 3. Excited-state diagrams illustrating the proposed mechanism for the photoreaction of $Ru(NH_3)_5py\text{-}X^{2+}$. k_i, internal conversion/intersystem crossing; k_n nonradiative deactivation.

F. Binuclear Complexes

Binuclear complexes have played an important part in various aspects of inorganic chemistry. Compounds have been formed in which the transition metal centers are connected by metal-metal bonds, bridging ligands, or with some combination of metal-metal bonds and bridging ligands.[15,16]

One aspect in which binuclear complexes have an important role is in the study of inner sphere electron transfer systems. In this process, the oxidant and the reductant share a ligand in their inner coordination spheres and the electron transfer occurs across the bridging ligand (equations 27-29).

Precursor formation:

$$\text{Ox-X} + \text{Red}(H_2O) \longrightarrow \text{Ox-X---Red} + H_2O \tag{27}$$

Activation and electron transfer:

$$\text{Ox-X---Red} \longrightarrow \text{Ox}^{-}\text{---X-Red}^{+} \tag{28}$$

Dissociation:

$$\text{Ox}^{-}\text{---X-Red}^{+} + H_2O \longrightarrow \text{Ox}(H_2O)^{-} + \text{X-Red}^{+} \tag{29}$$

The bridging ligand involved in this process can vary from a simple ligand, where a single atom serves as the bridge (such as halides, OR, SR, NR_2, and PR_2) to more complicated ligands (including organic bridges such as carboxylate or carboxamide complexes (examples 1 and 2)).

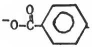

1

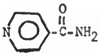

2

The rates of reaction depend on a variety of factors including steric effects of the bridge, the point of attack on the bridge, and the reducibility of the bridging ligand.[17]

Dissociation of the intermediate binuclear complex depends upon the substitutional lability or inertness of the metal ions involved. In equation (30), for example, the Cr(II) reactant is labile, with the

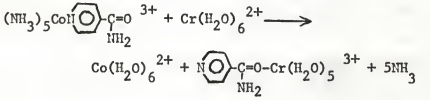

(30)

coordinated H_2O ligands undergoing rapid exchange with the solvent molecules. Upon transfer of an electron from Cr(II) to Co(III), the lability is also "transferred". The resulting Co(II) labilizes its ammine and bridging ligands, and thus the binuclear intermediate dissociates rapidly.[17,18]

In contrast to the rapid binuclear dissociation is the reaction shown in equation (31). Neither the Ru(II) nor the Cr(III) metal centers

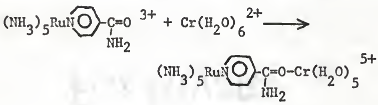

(:

in the binuclear product are very labile, so dissociation of the binuclear complex in solution occurs only slowly to give 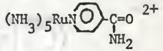 and $Cr(H_2O)_6^{3+}$.[17,18]

Another binuclear complex which has been extensively investigated is the mixed valence ion $(NH_3)_5Ru(pyz)Ru(NH_3)_5^{5+}$.[19,20] Interest in this complex has focused upon determination of the electronic structure of the ion. Two possibilities exist for the structure of the ground state.

The complex could have a symmetrical delocalized arrangement (conceptualized as $Ru^{2\frac{1}{2}+}$-pyz-$Ru^{2\frac{1}{2}+}$) or an unsymmetrical structure in which the metal ions are "trapped" in distinct oxidation states (Ru^{2+}-pyz-Ru^{3+}). Hush, et. al.[20], have reported results of near-infrared, infrared, and X-ray photoelectron spectra which are consistent with the symmetrical delocalized configuration for the ground state complex.

Recent studies[21] have also shown the ability of the dipositive ion pentaamminepyrazineruthenium(II), $Ru(NH_3)_5pyz^{2+}$, to act as a ligand and form binuclear complexes with various aqueous, first-row transition metal ions. Equilibrium studies have been reported on the complexes of nickel(II), copper(II), and zinc(II) with the $Ru(NH_3)_5pyz^{2+}$ ligand.[21] In addition, photo-induced intramolecular electron transfer studies have been performed on these complexes. Flash photolysis[22] of the $Ru^{II}(pyz)Cu^{II}$ complex results in transient bleaching of the MLCT band and this is believed to represent the photo-stimulated electron transfer to form $Ru^{III}(pyz)Cu^{I}$, followed by the redox regeneration of the starting material.

G. Nomenclature

A modification of the Ω convention[23] is used to designate the coordination sites of those bidentate ligands in which there may be uncertainty as to which position is bound to the metal in the complexes of this study. Since both coordinating sites of pyrazine are equivalent, no designation is needed for this ligand. 4-Cyanopyridine, on the other hand, can, potentially, coordinate at either the pyridine or the nitrile position.

In the Ω convention, the ligating atom is designated by its italic atomic symbol, preceded by the Greek letter Ω. This specification is placed directly after (and separated by a hyphen from) that portion of the ligand name which contains the ligating atom. Examples 3 and 4 illustrate the two possibilities for 4-cyanopyridine.

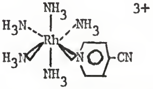

(4-cyanopyridine-Ω*N*)pentaamminerhodium(III)

3

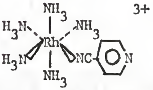

(4-cyano-Ω*N*-pyridine)pentaamminerhodium(III)

4

When the bidentate ligand bridges two metal centers, the atomic symbol of the metal to which the site is bound is included in parentheses following the ligating atom designation. The conventional use of μ to indicate a bridging ligand will also be included. Example 5

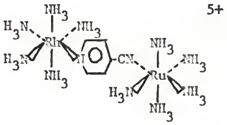

μ-(4-cyano-Ω*N*(Ru)-pyridine-Ω*N*(Rh))decaamminerhodium(III)ruthenium(II)

5

illustrates this method for a binuclear complex.

When a formula symbol is used to represent a complex, the 4-cyanopyridine abbreviation, pyCN, will be written such that the coordinating site is nearest the metal designated. For example, $[Rh(NH_3)_5pyCN]^{3+}$ indicates pyridine coordination, whereas $[Rh(NH_3)_5NCpy]^{3+}$ represents nitrile coordination. In the binuclear complex $[(NH_3)_5Rh(pyCN)Ru(NH_3)_5]^{5+}$, the rhodium metal center is bound to the pyridine position and the ruthenium is coordinated to the nitrile site.

H. Statement of the Problem

While many studies have been performed on intramolecular electron transfer precursors, little work has been done on binuclear intramolecular energy transfer reactions. Our aim was to develop a binuclear system which would undergo this type of energy transfer reaction.

Three major characteristics are important in developing this system. First, one of the bridged metals should have an absorption band which is highly absorbing but relatively nonreactive. Irradiation of the binuclear complex would be directed at this band. Second, the other metal should have bands of low extinction coefficients, but one the excited states should be highly reactive. Reaction of the binucl species would be expected from this state following excitation at the other center if the energy transfer is effective. Last, the excited states attributable to each of the metals should be at similar energies in order for the energy transfer to occur easily.

Various monomeric systems were reviewed to determine which could best be combined to form a binuclear system that would exhibit the intramolecular energy transfer. $Ru(NH_3)_5L^{2+}$ complexes have intense MLCT bands which would fulfill the first requirement of our plan of being highly absorbing. Variation of the ligand L can also result in the monomer being relatively nonreactive. $Rh(NH_3)L^{3+}$ complexes do not exhibit the MLCT bands characteristic of their ruthenium(II) homologs, but do have highly reactive, low absorbing LF bands. This type of monomer would fulfill the second requirement. In addition, these rhodium and ruthenium complexes have excited states at similar energy levels, which makes an intramolecular energy transfer feasible.

Pyrazine and 4-cyanopyridine were chosen as L ligands to bridge the Rh(III) and Ru(II) components to form two binuclear complexes. The spectra of both $[(NH_3)_5Rh(pyz)Ru(NH_3)_5][ClO_4]_5$ and $[(NH_3)_5Rh(pyCN)\text{-}Ru(NH_3)_5][ClO_4]_5$ exhibit MLCT bands, which are mostly $Ru^{II}L$ in character, occurring in the visible region. Internal ligand bands exhibited in the untraviolet region obscure the LF bands, attributable to the Rh(III) component, which are expected in that region.

Population of the MLCT excited state of the binuclear complexes is not expected to result in a significant amount of cleavage of the Ru-L bond due to the unreactive nature of the Ru(II) component. If an intramolecular energy transfer can occur from the Ru(II) to the Rh(III) after MLCT (Ru) irradiation, then the anticipated reaction would be cleavage of the Rh-L bond, the reaction which would be expected upon LF (Rh) irradiation. An intramolecular electron transfer is not expected to complicate the results since Rh(III) does not readily undergo redox reactions.[9]

EXPERIMENTAL

A. Materials

Rhodium trichloride trihydrate and ruthenium trichloride trihydrate were purchased from Matthey-Bishop, Inc., and were used without further purification. Reagent grade pyrazine and 4-cyanopyridine were used as obtained from Aldrich Chemical Company, Inc. Water used in syntheses, spectral determinations, and quantum yield determinations was redistilled from alkaline permanganate in an all glass apparatus. Purity of the complexes after recrystallization was determined, when possible, by comparison of their absorption spectra with published data.

B. Syntheses

1. Chloropentaamminerhodium(III) chloride, $[Rh(NH_3)_5Cl]Cl_2$: The procedure of Anderson and Basolo[24] was used. Three grams (0.11 mole) of $RhCl_3 \cdot 3H_2O$ was dissolved in 40 ml of water, followed by the addition of 10 g (0.187 mole) of ammonium chloride. 7.5 g (0.078 mole) of ammonium carbonate, which had been pulverized to a powder, was added slowly to the reaction mixture (due to immediate evolution of CO_2 and NH_3). The blood-red solution was heated in a hot water bath for three hours, during which time it turned to a yellow color. The solution was cooled and the golden yellow product which had formed was collected on a filter. The crystals were washed with approximately 125 ml of boiling hydrochloric acid: water (2:1 by volume) solution to remove the byproduct, trans-dichlorotetraamminerhodium(III) chloride (which dissolves in the hot 8 N HCl, but will precipitate when the filtrate is cooled). Then, the pale yellow product remaining on the filter was recrystallized from a minimum amount of boiling water, the filtrate was cooled, and

the crystals were collected, washed with ethanol then ether, and dried under vacuum.

Yield: 1.799 g (6.1 mole, 49.9%)

λ_{max} (nm), ε ($M^{-1}cm^{-1}$): 347, 95.6; 274, 113 (literature values[25]: 345, 102; 277, 109)

2. Aquopentaamminerhodium(III) perchlorate, $[Rh(NH_3)_5H_2O][ClO_4]_3$: This synthesis followed the procedure reported by Bushnell, et. al.[26] One-half gram of $[Rh(NH_3)_5Cl]Cl_2$ was added to 5 ml of 1 N NaOH in a small beaker. This solution was heated at 90° C for 30 minutes, after which it was cooled, and ~5 ml of concentrated perchloric acid was added to precipitate the fine white crystals of $[Rh(NH_3)_5H_2O][ClO_4]_3$. This product was collected, washed with ethanol then ether, and dried under vacuum.

Yield: 0.802 g (1.6 mmol, 94%)

λ_{max} (nm), ε ($M^{-1}cm^{-1}$): 316, 106; 262, 95 (literature values[9]: 316, 104; 263, 89)

3. Pentaamminepyrazinerhodium(III) perchlorate, $[Rh(NH_3)_5pyz]$-$[ClO_4]_3$: The method described by Creutz and Taube[19] was used for this synthesis. Aquopentaamminerhodium(III) perchlorate, 0.313 g (0.62 mmol), was dissolved in a solution containing 0.6 g (5.75 mmol) pyrazine in 5 ml dimethylformamide and placed in a 10 ml round bottom flask, which was fitted with a water-cooled condenser. The solution was heated in the dark at 90-100° in an oil bath for 28 hours. Dimethylformamide was stripped from the solution using a rotary evaporator, leaving a pale yellow oil behind. This oil was treated alternately with ethanol and ether, and the container was scratched with a glass rod until crystal

formation had been induced. The white crystals which formed were recrystallized from hot water, collected, and washed with ethanol then ether, and dried under vacuum.

Yield: 0.1085 g (0.19 mmol, 45.2%)

λ_{max} (nm), ε ($M^{-1}cm^{-1}$): 263, 0.59 x 10^4 (literature value[19]: 262, 0.596 x 10^4)

4. Chloropentaammineruthenium(III) chloride, $[Ru(NH_3)_5Cl]Cl_2$: This compound was synthesized following the method of Clarke[27]. Three grams (11.4 mmol) of ruthenium trichloride trihydrate was dissolved in 37 ml of water, and 30 ml of hydrazine hydrate (85%) was added slowly with stirring. This mixture was refluxed for 2 hours, then cooled. The golden yellow crystals which formed were collected and washed repeatedly with 1.5 N HCl to remove the ammonium chloride by-product. The product was recrystallized from hot 0.1 N HCl, and a large excess of concentrated HCl was added to the filtrate to cause precipitation. The crystals were collected, washed with ethanol then ether, and dried under vacuum.

Yield: 2.467 g (8.4 mmol, 73.5%)

λ_{max} (nm), ε ($M^{-1}cm^{-1}$): 327, 1470 (literature value[28]: 328, 1930)

5. μ-Pyrazinedecaamminerhodium(III)ruthenium(II) perchlorate, $[(NH_3)_5Rh(pyz)Ru(NH_3)_5][ClO_4]_5$: The method described by Creutz and Taube[19] was used for the synthesis of this compound. The apparatus for this synthesis is illustrated in Figure 4. A solution of 0.128 g (0.23 mmol) of pentaamminepyrazinerhodium(III) perchlorate in 4 ml of water was passed through a 5 cm column of Bio-Rad Anion Exchange Resin Dowex 1-X4 (200-400 mesh) in the chloride form. The eluates were

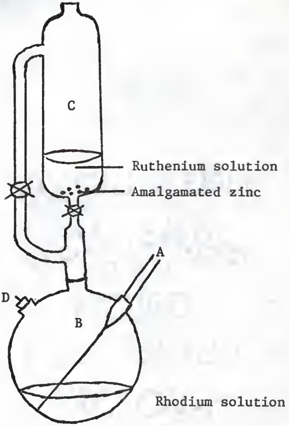

A: Argon inlet

B: Three-necked, round bottom flask

C: Pressure-equallizing dropping funnel

D: Stopper

Figure 4. Schematic diagram of apparatus used in the syntheses of binuclear complexes.

monitored spectrophotometrically to maintain a high concentration of the rhodium complex, and were then placed in the three-necked round-bottom flask.

Seven milliliters of 0.1 N sulfuric acid and 0.08 g (0.27 mmol) of chloropentaammineruthenium(III) chloride were combined with a few pieces of amalgamated zinc in the pressure-equalizing dropping funnel. Argon (scrubbed by passage through a Cr(II) solution) was bubbled into the rhodium solution and simultaneously through the ruthenium solution (by carefully opening the stopcock of the dropping funnel) for 0.5 hr. During this time, the ruthenium(III) was reduced to Ru(II) by the zinc amalgam, and the chloro ligand was labilized. The two solutions were then combined, and, within a short time after mixing, the pale yellow solution gradually turned a dark pink color. The flask was stored under argon at ~5° C overnight.

The following morning, the flask was opened to the air and 6 ml of saturated $NaClO_4$ was added to the solution. The flask was again cooled, and fine, dark purple crystals formed. The product was collected and washed with ethanol then ether, and dried under vacuum.

Yield: 0.0974 g (0.102 mmol, 45%)

λ_{max} (nm), ε ($M^{-1}cm^{-1}$): 528, 1.26×10^4; 264, 0.56×10^4 (literature values[19]: 528, 1.8×10^4; 263, 0.65×10^4)

6. (4-cyanopyridine-ΩN)pentaamminerhodium(III) perchlorate, $[Rh(NH_3)_5pyCN][ClO_4]_3$: This synthesis is a modification of the formation of pentaamminepyridinerhodium(III) perchlorate as described by Petersen, et. al.[9] Aquopentaamminerhodium(III) perchlorate, 0.2 g (0.4 mmol), and 8 ml of dimethylacetamide were combined in a round-

bottom flask which was fitted with a water-cooled condenser. This solution was heated in an oil bath at 100-110° C for 2 hours, then cooled to 85°. One gram (9.6 mmol) of 4-cyanopyridine was added, and the mixture was heated at 85° for another 6 hours. The hot solution was filtered through a prewarmed filter, then added to 100 ml of isobutanol, and the resulting suspension was cooled overnight. The white crystals which formed were collected, washed with ethanol then ether, and dried under vacuum. Carbon-13 NMR spectroscopy was used to confirm formation of the pyridine bound isomer.

Yield: 0.156 g (0.26 mmol, 65.6%)

λ_{max} (nm), ε ($M^{-1}cm^{-1}$): 259, 0.66×10^4

Anal: calculated for $[Rh(NH_3)_5pyCN][ClO_4]_5 \cdot H_2O$: N, 16.11%; C, 11.84%; H, 3.48%. Found: N, 15.94%; C, 11.84%; H, 3.76%.

7. (4-cyano-ΩN-pyridine)pentaammineruthenium(II) perchlorate, $[Ru(NH_3)_5NCpy][ClO_4]_2$: Note--ruthenium perchlorates are potentially explosive. They should be handled in small quantities and with caution. The procedure given by Clarke and Ford[29] was followed to prepare this compound. A solution of silver trifluoroacetate was made by dampening Ag_2O (0.06 g, 0.25 mmol) with 2 ml of water, and adding trifluoroacetic acid dropwise until most of the Ag_2O had dissolved. This solution was filtered into a beaker and digested with 0.1 g (0.34 mmol) of $[Ru(NH_3)_5Cl]Cl_2$. The mixture was filtered to remove the resulting AgCl and the filtrate was combined with 0.3 g (2.9 mmol) of 4-cyanopyridine, 0.5 g of amalgamated zinc, and trifluoroacetic acid to give $[H^+] \approx 0.5$ M. The dark reddish-purple solution which formed was stirred for 0.5 hr., then filtered. Saturated $NaClO_4$ solution was added to the filtrate to

precipitate reddish-brown crystals. The crude solid was recrystallized from a minimum of hot water, and the purified crystals obtained were washed with ethanol then ether, and dried under vacuum.

Yield: 0.07 g (0.14 mmol, 42%)

λ_{max} (nm), ϵ ($M^{-1}cm^{-1}$): 424, 0.784×10^4; 252, 1.15×10^4 (literature values[29]: 425, 0.537×10^4; 253, 0.891×10^4)

8. μ-(4-cyano-ΩN(Ru)-pyridine-ΩN(Rh))decaamminerhodium(III)-ruthenium(II) perchlorate, $[(NH_3)_5Rh(pyCN)Ru(NH_3)_5][ClO_4]_5$: The synthesis of this complex is a modification of the procedure given by Creutz and Taube[19] for the preparation of μ-pyrazinedecaamminerhodium-(III)ruthenium(II) perchlorate. The apparatus for this synthesis is illustrated in Figure 4. A 0.128 g (0.21 mmol) sample of (4-cyanopyridine-ΩN)pentaamminerhodium(III) perchlorate was dissolved in 5 ml of water, and was passed through a 5 cm column of Bio-Rad Dowex 1-X4 anion exchange resin in the chloride form. The eluates were monitored spectrophotometrically to maintain a high concentration of the complex. The rhodium complex solution was placed in the three-necked flask. $[Ru(NH_3)_5\text{-}Cl]Cl_2$, 0.08 g (0.27 mmol), was dissolved in 7 ml of 0.1 N sulfuric acid, and added to the pressure-equallizing dropping funnel which contained a few pieces of amalgamated zinc. Argon (scrubbed with Cr(II)) was bubbled into the rhodium solution and simultaneously through the ruthenium solution, by slightly opening the stopcock of the funnel, for 0.5 hr. During this time the ruthenium(III) was reduced to ruthenium(II) by the zinc amalgam, and the chloride ligand was labilized. The two solutions were then combined under argon, and, within a short time after mixing, the pale yellow solution gradually turned an intense purple color. The

flask was stored under argon at ~5° C overnight.

The next morning, the flask was opened to the air, and 3 ml of saturated $NaClO_4$ solution was added. The dark purple crystals which formed were collected on a sintered glass filter, washed with ethanol then ether, and dried under vacuum.

Yield: 0.158 g (0.16 mmol, 77%)

λ_{max} (nm), ε ($M^{-1}cm^{-1}$): 488, 0.946×10^4; 259, 1.39×10^4

Anal: calculated for $[(NH_3)_5Rh(pyCN)Ru(NH_3)_5][ClO_4]_5$: C, 7.39%; N, 17.23%; H, 3.49%. Found: C, 7.81%; N, 16.46%; H, 3.82%.

The remaining compounds described in this section were not characterized, and do not appear in the Results or Discussion sections.

9. 4-cyanopyridinium trifluoroacetate, $4\text{-NCpyH}^+\text{-CF}_3CO_2^-$: One gram (9.6 mmol) of 4-cyanopyridine was dampened slightly with water, then 1 ml of trifluoroacetic acid was added. The solution was stirred to dissolve all crystals. Additional small crystals of 4-cyanopyridine were added, one at a time, and dissolved, until a white precipitate began to form. The solution was cooled, then the product was collected, washed with a minimum of ether, and dried under vacuum.

Yield: 0.975 g (4.5 mmol)

10. Azidopentaamminerhodium(III) perchlorate, $[Rh(NH_3)_5N_3][ClO_4]_2$: This complex was synthesized following the procedure given by Reed, Gafney, and Basolo[30]. A 0.5 g (1.0 mmol) sample of $[Rh(NH_3)_5H_2O][ClO_4]_3$ was combined with 0.5 g of NaN_3 in 50 ml of water and heated at reflux for 1 hr. The volume of the solution was reduced to 5 ml, using a rotary evaporator, and 10 ml of a solution of 5% $NaClO_4$ in methanol was

added. The crude, yellow crystals which formed were recrystallized by dissolving in a minimum of hot water, then adding 5% $NaClO_4$ in methanol until the solution became turbid. The solution was cooled to ~0° C, and the yellow product which formed was collected, washed with methanol then ether, and dried under vacuum. During the synthesis, care was taken to prevent excessive exposure to light, and the fiber-like crystals obtained were stored in a vial covered with foil to prevent degradation by light.

Yield: 0.292 g (0.68 mmol, 68.6%)

λ_{max} (nm), ε ($M^{-1}cm^{-1}$): 334, 695; 250, 6930 (literature values[28]: 335, ~600; 250, ~5000)

11. (4-cyano-ΩN-pyridine)pentaamminerhodium(III) perchlorate, $[Rh(NH_3)_5NCpy][ClO_4]_3$: The synthesis of this compound was attempted from two different approaches, each giving a different result.

a. From aquopentaamminerhodium(III) perchlorate: This synthesis is a modification of a procedure described by Petersen[25] for the preparation of pentaamminepyridinerhodium(III) perchlorate. $[Rh(NH_3)_5H_2O]$-$[ClO_4]_3$, 0.2 g (0.4 mmol), was combined with 8 ml of dimethylacetamide and a few molecular sieves (Type-4A). The solution was heated at 100-110° for 2 hr. in a flask fitted with an air-cooled condenser. The solution was then cooled to 85°, and one gram of 4-cyanopyridinium trifluoroacetate was added. The temperature was maintained at 85° for an additional 4 hr., after which the solution was filtered to remove the molecular sieves, and added to 100 ml of isobutanol. The white suspension which formed was cooled at ~5° overnight. The following morning, the white crystals were collected and recrystallized by dissolving in a minimum of hot water and filtering into a saturated solution of $NaClO_4$ in methanol. The purified crystals were collected, washed with ethanol then ether, and dried under vacuum.

Yield (based upon desired product): 0.151 g (0.26 mmol, 64.5%)

λ_{max} (nm), ε ($M^{-1}cm^{-1}$): 318, 167; 262, 248

b. From azidopentaamminerhodium(III) perchlorate: A modification of the procedures given by Jordan, Sargeson, and Taube[31] was adapted for this synthesis. $[Rh(NH_3)_5N_3][ClO_4]_2$ (0.15 g, 0.35 mmol) was partially dissolved in 4 ml of triethylphosphate. 0.049 g (0.38 mmol) of $NOClO_4$ was initially added to the mixture. Then, additional small amounts of $NOClO_4$ were added until all of the rhodium-azide crystals had dissolved and reacted. After adding 0.32 g (1.5 mmol) of 4-cyanopyridinium trifluoroacetate, the solution was stirred at room temperature for 2 hours. The solution was added to 50 ml of ether to form a white suspension, which was cooled. The crude product was collected, washed with ether, and dried under vacuum.

Yield (based upon desired product): 0.085 g (0.2 mmol, 41%)

λ_{max} (nm), ε ($M^{-1}cm^{-1}$) (of unrecrystallized product): 313 (sh), 112; 275, 1173

12. μ-(4-cyano-ΩN(Rh)-pyridine-ΩN(Ru))decaamminerhodium(III)ruthenium(II) perchlorate, $[(NH_3)_5Rh(NCpy)Ru(NH_3)_5][ClO_4]_5$: The apparatus illustrated in Figure 5 was used in this synthesis. A 0.1 g (0.17 mmol) sample of what was believed to be $[Rh(NH_3)_5NCpy][ClO_4]_3$ (prepared from $[Rh(NH_3)_5H_2O][ClO_4]_3$) was dissolved in 5 ml of water and washed through a 5 cm column of Bio-Rad Dowex 1-X4 anion exchange resin in the chloride form. The eluates were monitored spectrophotometrically and placed in

the three-necked flask. $[Ru(NH_3)_5Cl]Cl_2$ (0.08 g, 0.27 mmol) was dissolved in 7 ml of 0.1 N sulfuric acid, and reduced over amalgamated zinc in the dropping funnel for 0.5 hr., while argon was bubbled through the apparatus. The two solutions were combined, and the resultant pale gold solution gradually turned a dark pink after approximately ten minutes. The flask was stored under argon at ~5° overnight.

The following morning, 3 ml of saturated $NaClO_4$ solution was added to the flask, which had been opened to the air. Additional cooling resulted in the formation of a dark purple precipitate. This crude product was collected, washed with ethanol then ether, and dried under vacuum. Attempts to recrystallize the product by dissolving in warm water and filtering into methanol saturated with $NaClO_4$ resulted in formation of crystals which, based on appearance and electronic spectral data, differed significantly from the crude product, and were assumed to have decomposed.

Yield (based on desired product): 0.077 g (0.08 mmol, 47%)

λ_{max} (nm), ε ($M^{-1}cm^{-1}$): 488, 380; 299, 962; 270, 909 (recrystallized product: 483, 180; 299, 764; 270, 727)

13. (4-cyanopyridine-ΩN)pentaammineruthenium(II) perchlorate, $[Ru(NH_3)_5pyCN][ClO_4]_2$: In an attempt to synthesize this compound, a modification of the procedure given by Clarke and Ford[29] for the formation of the nitrile bound isomer, was used. The modification appears to have been unsuccessful, resulting mainly in the formation of the nitrile bound isomer. Ag_2O (0.06 g, 0.25 mmol) was dampened with 3 ml of acetone, and trifluoroacetic acid was added dropwise until most of the Ag_2O had dissolved. $[Ru(NH_3)_5Cl]Cl_2$ (0.1 g, 0.34 mmol) was added

and digested at room temperature. AgCl did not precipitate out. The solution was filtered to remove any undissolved Ag_2O, then the filtrate was added to 0.3 g (2.9 mmol) of 4-cyanopyridine and 0.5 g of amalgamated zinc. The dark red solution which formed was stirred for 0.5 hr., then filtered. Saturated $NaClO_4$ solution was added to precipitate red-orange crystals, which were recrystallized from a minimum of hot water, washed with ethanol then ether, and dried under vacuum.

Yield (based on desired product): 0.024 g (0.05 mmol, 14.4%)

λ_{max} (nm), ε ($M^{-1}cm^{-1}$): 500 (sh), 0.442×10^4; 424, 0.766×10^4; 252, 1.16×10^4

C. Analyses

The elemental analyses of (4-cyanopyridine-ΩN)pentaamminerhodium(III) perchlorate, $[Rh(NH_3)_5pyCN][ClO_4]_3 \cdot H_2O$, and μ-(4-cyano-$\Omega N$(Ru)-pyridine-$\Omega N$(Rh))decaamminerhodium(III)ruthenium(II) perchlorate, $[(NH_3)_5Rh(pyCN)\text{-}Ru(NH_3)_5][ClO_4]_5$, were performed by Galbraith Laboratories, Inc., Knoxville, Tennessee.

D. Spectra

All ultraviolet and visible range absorption spectra were obtained with a Cary 14 Spectrophotometer. Spectra were recorded at room temperature on dilute solutions in redistilled water.

Infrared spectra were obtained as KBr pellets on a Perkin-Elmer 180 recording spectrophotometer. Approximately 1 mg of compound was combined with 100 mg of dry KBr and pulverized using a Wig-L-Bug Crescent amalgamator. The resultant powder was then formed into a pellet using a Wilks mini-press.

E. Photolysis Apparatus and Procedures

The optical train apparatus used in all photolysis reactions is illustrated by the schematic diagram in Figure 5. A 200-watt, mercury, short-arc lamp was used as the light source. An 8 cm quartz cell filled with water filtered out the infrared radiation, and an Oriel mercury line interference filter (G-521-2537, G-521-3130, G-522-4358, or G-522-5461) was used to isolate the desired wavelength. A hollow brass cell holder was used to thermostat the photolysis cells at 25° C.

Photolyses were carried out on aqueous perchloric acid solutions (pH = 2-4), which had been prepared gravimetrically in complex such that the optical density at the irradiation wavelength was ~1.5. Unless specified, the solutions were deoxygenated with chromous-scrubbed argon (using the apparatus illustrated in Figure 6) to prevent quenching of the excited state or oxidation of the ground state molecules by oxygen. The solutions were deoxygenated for a minimum of 0.5 hr. before filling and sealing the photolysis cells. Two- or ten-cm pathlength, cylindrical, quartz cells were used for the photolyses, with solution homogeneity maintained by periodically shaking the cells.

An identical dark reaction cell was prepared for each photolysis to correct for any thermal reactions. A Cary 14 Spectrophotometer was used to monitor the photolyses. To determine the quantum yield for the photosubstitution reactions, the absorbance spectra of the dark and the photolyzed solutions were recorded at the beginning and the end of the photolyses, and the difference spectra between the dark and the photolyzed solutions were recorded after each irradiation interval during the photolyses. Interval quantum yields were obtained from the absorbance

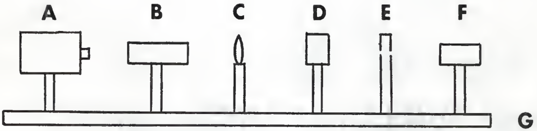

A	Light source
B	Infrared filter
C	Collimating lens
D	Wavelength selector
E	Light stop
F	Thermostated cell holder
G	Optical bench

Figure 5. Schematic diagram of optical train apparatus.

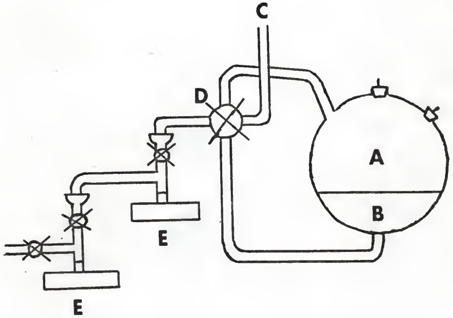

A	Zwickel flask
B	Solution
C	Argon inlet
D	Four-way stopcock
E	Photolysis cells

Figure 6. Schematic diagram of deoxygenation apparatus.

changes (at a preselected wavelength as well as the wavelength of irradiation) and the quantum yield values were plotted as a function of percent reaction. Extrapolation of this plot to zero percent reaction gave the initial quantum yield values for the photoaquation of the complexes reported, and eliminated complications resulting from secondary reactions. Calculations of interval quantum yields (according to equation 32) were carried out using the program in Appendix A, which was

$$\Phi = \frac{\text{moles of product}}{\text{einsteins absorbed}}$$

$$= \frac{C_L \cdot V}{I_o^i(1-10^{-\text{O.D.}})t} \tag{32}$$

where: C_L = concentration of product (in M)

V = volume of the cell (in ml)

I_o^i = intensity of the incident light

O.D. = average optical density at the irradiation wavelength

t = time (in min.)

written for a Hewlett-Packard model 9810A table-model calculator.

Quantum yields for the photoaquation of ammine ligands were calculated from the difference in pH of the photolyzed and dark solutions. The formula used for these calculations was

$$\Phi_{NH_3} = \frac{|\Delta n|}{I_o^i\ F\ t} \tag{33}$$

where $|\Delta n|$ is the change in the number of moles of H^+ as determined from the pH values of the dark and photolyzed solutions; I_o^i is the intensity of the incident light (ein./min.); F is the fraction of incident light absorbed ($F = 1 - \text{antilog}\ (-(A_{irr,0} + A_{irr,t})/2)$, where $A_{irr,0}$ is the absorbance at the irradiation wavelength at time zero, and $A_{irr,t}$ is the absorbance at the irradiation wavelength at time t); and t is the irradiation time. A Corning Model 5 pH Meter, which had been calibrated using commercial buffers, was used to obtain the pH measurements.

The incident intensity of the irradiation beam for each photolysis was determined by ferrioxalate[32] ($\lambda_{irr} \leq 436$ nm) or Reineckate salt[33] ($\lambda_{irr} \geq 436$ nm) actinometry. Typical values of I_o^i obtained were $1.3 \pm 0.1 \times 10^{18}$ quanta/min. ($\lambda_{irr} = 436$ nm), $\sim 9 \times 10^{16}$ quanta/min. ($\lambda_{irr} = 313$ nm), and $\sim 2 \times 10^{19}$ quanta/min. ($\lambda_{irr} = 546$ nm).

F. Carbon-13 NMR Spectra

Carbon-13 nuclear magnetic resonance spectra were obtained with a Varian XL-100-15 spectrometer operating at a frequency of 25.2 MHz and equipped with a Nicolet FT-100 Data System with quadrature phase detection and 20K of memory, allowing 16K data points, 8K points in the frequency domain for 3012 Hz spectral width. All spectra were measured on solutions saturated (~0.05 to 0.1 M) with complex and using D_2O/H_2O (1:1, v/v) as solvent. Dioxane was added as an internal standard. The flip angle was varied between 40 and 60° with a 7 second delay between pulses. The number of pulses required to obtain a good signal-to-noise ratio was 9520 for the spectrum of $[Rh(NH_3)_5pyCN][ClO_4]_3$.

RESULTS

A. Spectral Characteristics

1. Electronic spectra: The electronic absorption spectra of the complexes used in this research are listed in Table III.

The spectrum of $[Rh(NH_3)_5pyCN][ClO_4]_3$ is dominated by a peak occurring at 258 nm ($\varepsilon = 0.643 \times 10^4$ $M^{-1}cm^{-1}$). This coincides well with the $\pi^* \leftarrow \pi$ band in the spectrum of 4-cyanopyridine free ligand (λ_{max} = 275 nm, $\varepsilon = 0.341 \times 10^4$ $M^{-1}cm^{-1}$). In addition, other $Rh(NH_3)_5L^{3+}$ complexes, in which L is an unsaturated heterocycle, display similar peaks which have been assigned as internal ligand transitions[9]. Both of the lower intensity ${}^1E^b, {}^1B_2 \leftarrow {}^1A_1$ and ${}^1E^a, {}^1A_2 \leftarrow {}^1A_1$ ligand field transitions, which are expected to occur in the same spectral region, are obscured by the highly intense IL band.

The electronic spectrum of $[Ru(NH_3)_5NCpy][ClO_4]_2$ exhibits MLCT (λ_{max} = 425 nm, $\varepsilon = 0.537 \times 10^4$ $M^{-1}cm^{-1}$) and IL (λ_{max} = 253 nm, ε = 0.891×10^4 $M^{-1}cm^{-1}$) bands which are characteristic of other $Ru(NH_3)_5L^{2+}$ complexes[34,35]. Protonation of the pyridine site enhances the π-acceptor ability of the 4-cyanopyridine ligand and shifts the MLCT band to a longer wavelength (λ_{max} = 532 nm, $\varepsilon = 0.831 \times 10^4$ $M^{-1}cm^{-1}$)[31]. Coordination of $Rh(NH_3)_5^{3+}$ to the pyridine nitrogen of this ligand would also increase the electron-withdrawing ability of the ligand. Thus, the MLCT band of $Ru(NH_3)_5NCpy^{2+}$ is expected to red shift upon formation of the Rh^{III}-pyCN-Ru^{II} binuclear complex. This perturbation is observed, with the MLCT band occurring at 488 nm ($\varepsilon = 1.32 \times 10^4$ $M^{-1}cm^{-1}$).

In a similar manner, coordination of $Rh(NH_3)_5^{3+}$ to pyrazine increases that ligand's π electron-acceptor nature. This causes the MLCT band associated with the $Ru(NH_3)_5pyz^{2+}$ moiety (λ_{max} = 472 nm[8]) to shift

Table III. Electronic Absorption Spectra of Various Rhodium and Ruthenium Ammine Complexes.

Complex	λ_{max}[a]	ε_{max}[b]	Assignment	Ref.
$[Rh(NH_3)_5Cl]Cl_2$	345	103	${}^1E^a, {}^1A_2 \leftarrow {}^1A_1$	25
	277	109	${}^1E^b, {}^1B_2 \leftarrow {}^1A_1$	
$[Ru(NH_3)_5Cl]Cl_2$	328	1930	${}^1E^a, {}^1A_2 \leftarrow {}^1A_1$	28
$[Rh(NH_3)_5H_2O][ClO_4]_3$	316	104	${}^1E^a, {}^1A_2 \leftarrow {}^1A_1$	9
	263	89	${}^1E^b, {}^1B_2 \leftarrow {}^1A_1$	
$[Rh(NH_3)_5pyz][ClO_4]_3$	262	0.596×10^4	IL	19
$[(NH_3)_5Rh(pyz)Ru(NH_3)_5][ClO_4]_5$	528	1.8×10^4	MLCT	19
	263	0.65×10^4	IL	
$[Rh(NH_3)_5pyCN][ClO_4]_3$	285(sh)	0.30×10^4	(IL)	c
	276(sh)	0.48×10^4	(IL)	
	258	0.643×10^4	IL	
$[(NH_3)_5Rh(pyCN)Ru(NH_3)_5][ClO_4]_5$	488	1.32×10^4	MLCT	c
	258	1.77×10^4	IL	
$[Ru(NH_3)_5NCpy][ClO_4]_2$	425	0.537×10^4	MLCT	29
	253	0.891×10^4	IL	
$[Rh(NH_3)_5N_3][ClO_4]_2$	335	590	LF	28
	251	5200	IL	

[a] in nanometers
[b] in $M^{-1}cm^{-1}$
[c] this work

to a longer wavelength upon formation of the Rh^{III}-pyz-Ru^{II} binuclear species (λ_{max} = 528 nm).

2. Infrared spectra: Table IV summarizes the nitrile stretching frequencies observed for the complexes of this study. For those complexes in which a CN stretch could not be resolved, the decrease in intensity of the peak may have been a result of coordination of the ligand to the metal center[36], or due to a failure in the synthesis of the compound.

Two ν(CN) peaks are observed in the spectrum of $[Ru(NH_3)_5NCpy]$-$[ClO_4]_2$. This is a result of formation of both the pyridine and the nitrile bound isomers of the complex. The strong peak at 2179 cm^{-1} corresponds to the nitrile-bound isomer and is 60 cm^{-1} lower in frequency than the free ligand band due to π-back-bonding of Ru(II) into the nitrile group[29,34,37]. The smaller decrease from the free ligand frequency of the weaker peak at 2225 cm^{-1} is consistent with the previously characterized pyridine-bound complex[29].

3. Carbon-13 nuclear magnetic resonance: An attempt was made to determine NMR spectra on $[Rh(NH_3)_5pyCN][ClO_4]_3$, $[Rh(NH_3)_5NCpy][ClO_4]_3$, $[Ru(NH_3)_5NCpy][ClO_4]_2$, and $[(NH_3)_5Rh(pyCN)Ru(NH_3)_5][ClO_4]_5$. Of these, only $[Rh(NH_3)_5pyCN][ClO_4]_3$ provided a spectrum where the signals were distinguishable from noise. The chemical shifts and assignments of this spectrum are summarized in Table V. The down field shifts of the α, β, and γ carbon atoms of the 4-cyanopyridine, relative to the free ligand, are typical of metal bound pyridine derivatives where little or no π-back-bonding is evident[36,38].

The two Ru(II)-containing complexes, which gave no carbon-13 signals, may have been contaminated with Ru(III). The presence of even a small

Table IV. Nitrile stretching frequencies of various rhodium and ruthenium ammine complexes.

Compound	ν(CN), cm^{-1a}
4-cyanopyridine (free ligand)	2239 m, sharp
$[Rh(NH_3)_5pyCN][ClO_4]_3$	2238 w
$[Rh(NH_3)_5NCpy][ClO_4]_3$	
a. From aquo complex	ND
b. From azido complex	ND
$[Ru(NH_3)_5NCpy][ClO_4]_2$	2179 s, sharp
$([Ru(NH_3)_5pyCN][ClO_4]_2$	2225 w, sharp
$[(NH_3)_5Rh(pyCN)Ru(NH_3)_5][ClO_4]_5$	2166 m, sharp
$[(NH_3)_5Rh(NCpy)Ru(NH_3)_5][ClO_4]_5$	ND

[a] Abbreviations: s, strong; m, medium; w, weak; ND, not distinguishable from noise.

Table V. ^{13}C nuclear magnetic resonance chemical shifts of $[Rh(NH_3)_5pyCN][ClO_4]_3$ and 4-cyanopyridine, free ligand.

	Free ligand[b]	Rh complex[c]	$\Delta\delta$[d]
α	150.5	153.9	+3.4
β	127.0	130.7	+3.7
γ	121.4	125.1	+3.7
C≡N(δ)	117.6	116.0	-1.6

[a] 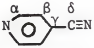

[b] Reference 37

[c] Relative to TMS using dioxane as internal standard ($\delta_{(^{13}CH_3)_4Si} = \delta_{^{13}C_4H_8O_2} + 67.40$)

[d] $\delta_{complex} - \delta_{free\ ligand}$

amount of this paramagnetic substance would cause a decrease in T_1 (spin-lattice relaxation time) and could result in considerable broadening of the signals. Lack of signals from $[Rh(NH_3)_5NCpy][ClO_4]_3$ may have been due to a failure in the synthesis of this complex.

B. Photolyses

Table VI summarizes the irradiation wavelengths and resultant quantum yield values for the specifies reactions obtained upon irradiation of various complexes in this study.

1. Photolysis of $[Rh(NH_3)_5pyz][ClO_4]_3$: A solution of $[Rh(NH_3)_5pyz]$-$[ClO_4]_3$ (1.87×10^{-3} $\underline{M}$ in non-deoxygenated pH 2 $HClO_4$) was irradiated at 313 nm for 60 min. ($I_o^i = 4.32 \times 10^{17}$ quanta/min.). This irradiation wavelength corresponded to the low energy tail of the IL band of the complex. LF bands which occur in the same spectral region are obscured by the more intense IL band, so that, presumably, there is population of both IL and LF excited states upon irradiation. If this photolysis were to result in photoaquation of the unique ligand and formation of $Rh(NH_3)_5$-H_2O^{3+}, the characteristic reaction of other $Rh(NH_3)_5L^{3+}$ complexes[9], a decrease in the absorbance at the monitored wavelength of 316 nm would be expected. This, however, was not observed. The absorbance at 316 nm increased substantially, and the actual photoproduct has not, as yet, been identified. If, however, a significant amount of light was absorbed into the IL bands, pyrazine (either complexed or the free ligand formed from photoaquation) could break down through a ring opening process similar to the reaction observed for pyridine[39]. Calculation of a quantum yield requires that the product be known; therefore, no Φ values

Table VI. Irradiation wavelengths and quantum yields for the complexes photolyzed.

Compound	λ_{irr} (nm)	Φ (moles/ein.)
$[Rh(NH_3)_5pyz][ClO_4]_3$	313	a
$[(NH_3)_5Rh(pyz)Ru(NH_3)_5][ClO_4]_5$	436	$7.3 \pm 0.7 \times 10^{-5}$ (2)[b]
	546	$2.80 \pm 0.04 \times 10^{-6}$ (2)[b]
$[Rh(NH_3)_5pyCN][ClO_4]_3$	313	$9.8 \pm 0.1 \times 10^{-2}$ (2)[c]
$[Ru(NH_3)_5NCpy][ClO_4]_2$	436	$2.03 \pm 0.29 \times 10^{-2}$ (2)[c]
$[(NH_3)_5Rh(pyCN)Ru(NH_3)_5][ClO_4]_5$	436	$1.06 \pm 0.16 \times 10^{-3}$ (5)[d]

[a] product unknown

[b] disappearance of starting material

[c] loss of 4-cyanopyridine ligand

[d] Rh-pyCN bond breaking

could be determined for this photolysis.

2. Photolysis of $[(NH_3)_5Rh(pyz)Ru(NH_3)_5][ClO_4]_5$: A deoxygenated solution of $[(NH_3)_5Rh(pyz)Ru(NH_3)_5][ClO_4]_5$, which was ~6 x 10^{-6} M in pH 4 $HClO_4$, was prepared for irradiation at 436 nm (I_o^i = 3.3 x 10^{18} quanta/min.) and at 546 nm (I_o^i = 2.1 x 10^{19} quanta/min.). Both of these wavelengths are included in the MLCT envelope of the complex. A teflon stirring bar was used in each photolysis cell to maintain homogeneity of the solution. Limiting quantum yields for disappearance of the starting material were determined based upon the absorbance change observed over the total irradiation time of 60 min. At λ_{irr} = 436 nm, the quantum yield was 7.3 ± 0.7 x 10^{-5} (2) moles/ein. (~4% reaction), and at λ_{irr} = 546 nm, the quantum yield after 3.6% of reaction was 2.80 ± 0.04 x 10^{-6} (2) moles/ein.

3. Photolysis of $[Rh(NH_3)_5pyCN][ClO_4]_3$: A 2.7 x 10^{-3} M (pH 2 $HClO_4$) solution of $[Rh(NH_3)_5pyCN][ClO_4]_3$ (not deoxygenated) was irradiated at 313 nm for 60 min. (I_o^i = 2.7 x 10^{17} quanta/min.). This irradiation wavelength is on the lower energy tail of the intense peak which has been assigned as an IL transition. The photolysis may have resulted in a small amount of direct population of LF excited states if the $^1E^a$, $^1A_2 \leftarrow {}^1A_1$ transition is obscured by the IL peak in this spectral region.

During the photolysis, the absorbance at the monitored wavelength of 316 nm decreased. This is consistent with the reaction being photoaquation of the 4-cyanopyridine. The photolysis was taken to ~8% of reaction, and a quantum yield of 9.8 ± 0.1 x 10^{-2} (2) moles/ein. was determined, following thermal correction and extrapolation to 0% reaction.

4. Photolysis of $[Ru(NH_3)_5NCpy][ClO_4]_2$: Irradiation of $[Ru(NH_3)_5NCpy][ClO_4]_2$ (9×10^{-6} $\underline{M}$ in pH 4 $HClO_4$) at 436 nm ($I_o^i = 1.15 \times 10^{18}$ quanta/min.) resulted in photoaquation with $\Phi_{NCpy} = 2.03 \pm 0.29 \times 10^{-2}$ (5) moles/ein. The quantum yield for ammine aquation, as measured by pH change, exhibited a wide variation, since the compound is air sensitive. The average value of Φ_{NH_3} was ~0.1 moles/ein., but is considered to be unreliable.

5. Photolysis of $[(NH_3)_5Rh(pyCN)Ru(NH_3)_5][ClO_4]_5$: A solution of $[(NH_3)_5Rh(pyCN)Ru(NH_3)_5][ClO_4]_5$ ($\sim 1 \times 10^{-5}$ $\underline{M}$ in pH 4 $HClO_4$) was prepared for irradiation at 436 nm, a wavelength included in the MLCT envelope of the complex. The incident intensity of the light beam was $\sim 1.3 \times 10^{18}$ quanta/min. The photolyses generally featured an increase in absorbance at 425 nm (the λ_{max} for $Ru(NH_3)_5NCpy^{2+}$) and decreases at 510 and 260 nm. Isosbestic points were formed in the region of ~350 and ~460 nm, but these points were generally maintained for only 10-12 minutes of irradiation (~7% reaction). Continued irradiation resulted in a decrease in the absorbance which had initially increased at 425 nm, until ultimately the spectrum resembled the spectrum of free 4-cyanopyridine. The initial quantum yield value for the disappearance of the starting material was $1.06 \pm 0.16 \times 10^{-3}$ (5) moles/ein. The Φ_{NH_3} value, as determined from pH change, was $2.93 \pm 0.72 \times 10^{-1}$ (2).

As an aid in determining the photoproducts resulting from irradiation of the Rh^{III}-pyCN-Ru^{II} binuclear complex, ion exchange analyses of $[Ru(NH_3)_5NCpy][ClO_4]_2$ were performed. In the first analysis, 6 ml of a 2.76×10^{-5} $\underline{M}$ solution of $[Ru(NH_3)_5NCpy][ClO_4]_2$ were deposited onto a 5 cm column of Dowex 50W-X4 Cation Exchange Resin (200-400 mesh) in the H^+

form, which had previously been washed with redistilled water. The complex was eluted from the column with 3 $\underline{M}$ NaCl, and 10 ml aliquots were collected. The spectrum of each aliquot was recorded, with the first and second aliquots eluted showing a peak at ~335 nm. This peak corresponds fairly well to that expected for $Ru(NH_3)_5Cl^{2+}$ (λ_{max} = 328 nm, ε = 1930 $M^{-1}cm^{-1}$)[40], a complex which could be formed as a result of oxidation of the metal by oxygen, followed by anation with the Cl^- ions present.

The second ion exchange analysis was performed on the same H^+ resin column which was used in the first analysis, with the resin having been washed with 1 $\underline{M}$ $HClO_4$. Six milliliters of 2.76 x 10^{-5} $\underline{M}$ $[Ru(NH_3)_5$-$NCpy][ClO_4]_2$ were deposited onto the column. Immediately, the solution changed from a reddish-orange to a purple color, corresponding to protonation of the pyridine site. The complex was washed through the column with 3 $\underline{M}$ $NaClO_4$, and 10 ml aliquots were collected. The spectrum of the first aliquot contained a peak at ~260 nm, and the spectra of the second and third aliquots displayed peaks at ~355 nm. The peak at ~260 nm corresponds well with $Ru(NH_3)_5H_2O^{3+}$ (λ_{max} = 268 nm, ε = 635 $M^{-1}cm^{-1}$) [41]. This complex could result from oxidation of the metal center by oxygen, and aquation of the 4-cyanopyridine ligand. The peak at ~355 nm does not coincide well with any anticipated products and has not, as yet, been identified.

An ion exchange analysis was performed to determine the initial products resulting from the photolysis of $[(NH_3)_5Rh(pyCN)Ru(NH_3)_5][ClO_4]_5$. An 8.2 x 10^{-5} $\underline{M}$ solution (pH 4 $HClO_4$, deoxygenated) of the binuclear complex was irradiated at 436 nm in a 2 cm cell until ~39% of the reaction had been completed. This solution was then deposited onto a 5 cm column of Dowex 50W-X4 Cation Exchange Resin (200-400 mesh) in the H^+ form. The resin was washed with 3 M NaCl and 10 ml aliquots were collected. The spectrum of the first aliquot contained a peak at 332 nm, and aliquots 4-8 featured peaks at 258 and 488 nm. This ion exchange behavior is similar to that observed for $Ru(NH_3)_5NCpy^{2+}$. Decomposition of the material on the column, however, prevents direct comfirmation of the primary photolysis step.

DISCUSSION

A. 4-Cyanopyridine Complexes of $Fe(CN)_5^{3-}$, $Ru(NH_3)_5^{2+}$, $Co(CN)_5^{2-}$, and $Rh(NH_3)_5^{3+}$

4-Cyanopyridine complexes of pentacyanoferrate(II)[36], pentacyanocobaltate(III)[36], and pentaammineruthenium(II)[29] have previously been prepared. In this study, we have prepared and characterized the 4-cyanopyridine complex of the analogous pentaamminerhodium(III).

Similarities in absorption spectra have been observed between the cyano complexes of the first row transition metals and the ammine complexes of the second row metals for MA_5pyX homologs[42]. The spectra of $Co(CN)_5L^{2-}$ complexes exhibit bands or shoulders in the ultraviolet region which have been assigned to LF ($^1E^a$, $^1A_2 \leftarrow {}^1A_1$) transitions[36]. Peaks of similar origin occur in the same region in spectra of various $Rh(NH_3)_5L^{3+}$ complexes[9], although these transitions are obscured by the IL band in the Rh(III)-4-cyanopyridine complex. These ligand field bands are relatively insensitive to the nature of the L ligand.

The spectra of the $Fe(CN)_5L^{3-}$ and $Ru(NH_3)_5L^{2+}$ complexes exhibit intense MLCT bands in the visible-near ultraviolet region of the spectrum. In contrast to the peaks of the Co(III) and Rh(III) complexes, these MLCT bands are highly sensitive to the nature of the L ligand.

An interesting feature in the 4-cyanopyridine complexes of these four transition metal ions is the coordination site preferences exhibited by the metal centers. Like $Co(CN)_5^{2-}$ and $Fe(CN)_5^{3-}$, $Rh(NH_3)_5^{3+}$ favors the formation of the pyridine-bound isomer with the 4-cyanopyridine ligand. The coordination site of the Rh(III) complex is confirmed by the downfield shifts of the α, β, and γ carbons and the upfield shift of the δ carbon, with respect to the free ligand, in the ^{13}C NMR spectrum of this complex[38].

In addition to the difference in basicity of the two sites of the 4-cyanopyridine ligand, two other factors are important in determining the structural preferences displayed by this series of complexes. First, the pyridine nitrogen of the ligand is more sterically hindered (due to the protons on the α carbons) than the nitrile position. Therefore, coordination at the pyridine site would be favored in complexes where neighboring ligands are small enough to create relatively little steric hindrance. Cyano ligands are sterically less hindering than ammine groups; thus, the $Fe(CN)_5^{3-}$ and $Co(CN)_5^{2-}$ complexes are expected to favor pyridine coordination, and the $Ru(NH_3)_5^{2+}$ and $Rh(NH_3)_5^{3+}$ would prefer nitrile coordination. The Rh(III) complex, however, does not bind to the nitrile nitrogen as is expected from the steric hindrance.

A second factor which influences the site of complex coordination is the nature of the solvent. In an aqueous solution, stronger hydrogen bonding occurs between the water molecules and the pyridine nitrogen than the nitrile nitrogen of the 4-cyanopyridine. This, in effect, inhibits coordination to a metal center at the pyridine site. Of the four homologs, only the synthesis involving $Rh(NH_3)_5^{3+}$ is performed in a nonaqueous solvent (dimethylacetamide). In DMA, there is no hydrogen bonding to inhibit the pyridine site from Rh(III), and coordination of the metal is expected at this more basic position. The Fe(II), Co(III), and Ru(II) complexes are prepared in aqueous solutions, and have substantial hydrogen bonding at the pyridine nitrogen. On the basis of hydrogen bonding, we might expect the Fe(II), Co(III), and Ru(II) complexes to preferentially bind the nitrile position.

Both the $Fe(CN)_5^{3-}$ and $Co(CN)_5^{2-}$ complexes have conflicting

4-cyanopyridine coordination influences. Their smaller cyano ligands suggest a preference for a pyridine-bound complex, whereas the use of water as a solvent in the synthetic reactions leads us to expect a nitrile-bound isomer. For both metal systems, the pyridine-bound isomer is formed. Thus, in these cases, the lesser steric hindrance, in addition to the pyridine basicity, is the predominant factor in determining the most stable species.

The $Rh(NH_3)_5^{3+}$ complex also has conflicting factors affecting coordination to the 4-cyanopyridine ligand. The neighboring ammine groups favor nitrile coordination (from steric considerations), while the nonaqueous solvent used in the synthesis would suggest a preference for complexation to the pyridine site (lack of hydrogen bonding). In this case, the availability of the more basic pyridine position is favored in determining the most stable product.

The synthesis procedure for the $Ru(NH_3)_5^{2+}$ complex ion has both the steric factor and the solvent effect contributing to a preference for nitrile coordination. Synthesis of the complex results mainly in formation of the nitrile-bound isomer, yet a small amount of the pyridine-bound isomer is also detected[29]. Therefore, the greater basicity of the pyridine site nearly offsets the factors of steric hindrance and solvation which lead predominantly to nitrile coordination. (Reactions of $Ru(NH_3)_5H_2O$ and 4-cyanopyridine in nonaqueous solvents results in the major product being the pyridine-bound isomer[43]).

B. Photolyses

The MLCT band of $[Ru(NH_3)_5NCpy][ClO_4]_2$ occurs at 425 nm. If this complex can be compared to Ford's Ru^{II}-pyX species[13], then it is expected to be "reactive". The quantum yield for photoaquation of L of $2.03 \pm 0.29 \times 10^{-2}$ moles/ein., which was determined for this complex, is consistent with this expectation.

Protonation of the $Ru(NH_3)_5NCpy^{2+}$ species shifts the MLCT band to 532 nm[29]. Similarly, coordination of the positively charged $Rh(NH_3)_5{}^{3+}$ group increases the ligand's electronegativity toward Ru(II), and red shifts the MLCT band to 488 nm. This places the Rh^{III}-pyCN-Ru^{II} binuclear complex in a borderline position between the "reactive" and the "unreactive" categories.

Irradiation of the Rh-pyCN-Ru^{5+} complex initially showed an increase in absorbance at 425 nm, the λ_{max} for $Ru(NH_3)_5NCpy^{2+}$. This product is consistent with initial cleavage of the Rh(III)-L bond. Irradiation of the binuclear complex was at 436 nm, a wavelength too low in energy to populate a ^{1}LF (Rh) state. Since the Rh(III) ^{3}LF is assumed to be the lowest excited state and, thus, responsible for the photoreactions in the Rh(III) monomeric systems[8], indirect population of this state could be responsible for the photolysis product observed upon irradiation of the binuclear complex. If the Ru(II) ^{1}MLCT and the Rh(III) ^{3}LF states of the binuclear complex are at similar energy levels, an energy transfer or intramolecular sensitization could occur from the ^{1}MLCT state to the ^{3}LF (Rh(III)) state.

To test this mechanism, we have performed energy level calculations to determine the feasibility of this intramolecular energy transfer. Since emission data for the monomer components of the binuclear complex have not been obtained, these calculations were based on related or analogous complexes and, therefore, can only result in approximate energy level values.

Energies of the LF transitions in a d^6 octahedral complex can be calculated from crystal field theory according to the following equations[44]:

$$E(^1T_{1g} \leftarrow {}^1A_{1g}) = 10Dq - C + 86B^2/10Dq \tag{34}$$

$$E(^1T_{2g} \leftarrow {}^1A_{1g}) = 10Dq + 16B - C + 2B^2/10Dq \tag{35}$$

$$E(^3T_{1g} \leftarrow {}^1A_{1g}) = 10Dq - 3C + 50B^2/10Dq \tag{36}$$

$$E(^3T_{2g} \leftarrow {}^1A_{1g}) = 10Dq + 8B - 3C + 14B^2/10Dq \tag{37}$$

where 10Dq is the energy separation between the t_{2g} and the e_g levels, and B and C are Racah parameters dealing with electronic repulsions. The last term in equation (34) is generally small and can be ignored, giving equation (38):

$$\tilde{\nu} = 10Dq - C \tag{38}$$

where $\tilde{\nu}$ is the maximum of the $^1T_{1g} \leftarrow {}^1A_{1g}$ transition in the absorbance spectrum of a low spin d^6 octahedral complex[18]. In cases where there is insufficient data to determine the value of C, it can be approximated[44] by assuming that

$$C \simeq 4B \tag{39}$$

Reduction of the symmetry to D_{4h} or C_{4v}, by introducing one or two axial ligands, removes the degeneracy of the T states with T_{1g} reducing to E^a and A_2, and T_{2g} becoming E^b and B_2. When the axial ligand(s) is (are) weaker field (Dt > 0), the $E(T_1)$ state is lowest in energy in both the singlet and triplet manifolds.

$$E(^1A_2 \leftarrow {}^1A_1) = 10Dq - C \tag{40}$$

$$E(^1E^a \leftarrow {}^1A_1) = 10Dq - C - (35/4)Dt \tag{41}$$

$$E(^3A_2 \leftarrow {}^1A_1) = 10Dq - 3C \tag{42}$$

$$E(^3E^a \leftarrow {}^1A_1) = 10Dq - 3C - (35/4)Dt \tag{43}$$

The absorption spectrum of $Ru(NH_3)_5acn^{2+}$ (acn = acetonitrile) has a band at 350 nm (28.6 kK) which has been assigned to a ${}^1E^a({}^1T_1) \leftarrow {}^1A_1$ transition[34]. Using B = 0.42 kK (for $Ru(en)_3^{2+}$ [44]) and equations (39) and (41), a value of 10Dq - (35/4)Dt = 30.3 kK is determined for $Ru(NH_3)_5acn^{2+}$. This is also taken as the approximate value of 10Dq - (35/4)Dt for $Ru(NH_3)_5NCpy^{2+}$. Substituting into equation (43) gives:

$$\begin{aligned} E({}^3E^a \leftarrow {}^1A_1) &= 10Dq - 3C - (35/4)Dt \\ &= 30.3 - 3(4)(0.42) \\ &= 25.3 \text{ kK} \end{aligned} \tag{44}$$

Since the ground state and the excited state generally have slightly different internuclear distances at equilibrium, the energy of absorption would be for a transition from the 0 vibration level of the ground state to a higher vibrational level in the excited state (Figure 7). The 0-0 transition energy is obtained by subtracting half the Stokes Shift (energy difference between absorbance and emission) from the energy of absorption. When absorption and emission data are not available for the same excited state, the 0-0 energy must be approximated[9]. Assuming that the Stokes Shift for Ru(II) would be similar to that of Rh(III) (1/2 Stokes Shift = ~4.5 kK[9]), we conclude that the energy of the ${}^3LF$ state, relative to the ${}^1A_1$ ground state, is in the range of 20-21 kK.

An energy manifold for the ${}^1CT$ state was determined for $(NH_3)Rh(pyCN)Ru(NH_3)_5^{5+}$ from the electronic absorption spectrum. This range of energy levels includes most of the vibrational transitions possible in the formation of the ${}^1CT$ excited state. The approximate upper and lower wavelength limits for the envelope of the charge transfer band were used to specify the upper and lower limits of the energy manifold.

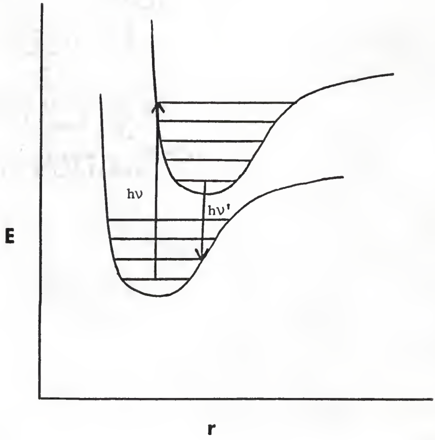

hν: energy of absorption

hν': energy of emission

Figure 7. Potential energy curve illustrating the excitation of a ground state molecule.

Since the ^{1}CT band of $(NH_3)_5Rh(pyCN)Ru(NH_3)_5^{5+}$ extends from ~400 nm to ~600 nm, the upper and lower energy limits for the manifold are 25 kK and 17 kK, respectively.

Emision studies have been reported on several Rh(III) complexes[9]. It was observed that the energy of the lowest excited state (assumed to be $^3T_1$ in octahedral microsymmetry) decreased with decreasing Brönsted basicity of the ligand[9]. Coordination of the $Ru(NH_3)_5^{2+}$ group to the nitrile position of the 4-cyanopyridine ligand increases the pK_a from 1.9 to 2.72 for the pyridine nitrogen (π-back-bonding ability of the dipositive metal overwhelms the opposing sigma withdrawal to result in net increase of pK_a)[29]. Comparison of this pK_a for the Ru^{II}-NCpy ligand with other $Rh(NH_3)_5L^{3+}$ complexes[9] leads us to expect the energy of the Rh(III) $^3T_1$ state to be near 20 kK.

Figure 8 illustrates the energy level diagram as calculated for the proposed Rh^{III}-pyCN-Ru^{II} energy transfer mechanism. The ruthenium ^{3}LF energy level differs in positioning from that proposed by Ford[13], where the energies of the LF states were estimated from $Ru(NH_3)_6^{2+}$. Using 10Dq = 27.1 kK for the hexaammine complex[45] and equations (34) and (36), the approximate values for ^{1}LF and ^{3}LF are 21.0 and 17.4 kK, respectively.

Application of present theory concerning MLCT transitions is inadequate[44] to determine the energy of a ^{3}CT level. Emission studies performed on a variety of ruthenium(II) complexes[46] show the lowest lying excited state to be a manifold of charge transfer levels. Therefore, a ^{3}CT state (the spin multiplicity may be meaningless due to spin-orbit coupling) would occur at an energy below the ^{3}LF and ^{1}CT levels in Figure 8.

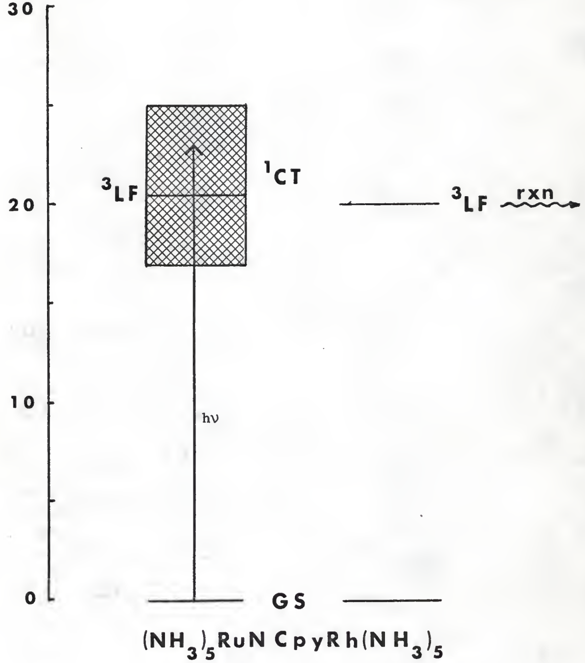

Figure 8. Energy level diagram for $(NH_3)_5Ru(NCpy)Rh(NH_3)_5^{5+}$. hν corresponds to irradiation at 436 nm.

An intramolecular energy transfer from the ^{3}CT (Ru) state to the ^{3}LF (Rh) following irradiation into the ^{1}CT manifold appears to be unlikely due to the endergonic nature of the process. An energy partitioning could occur, however, with competition between $^1\text{CT} \rightarrow {}^3\text{LF}$ (Rh) and $^1\text{CT} \rightarrow {}^3\text{LF}$ (Ru),^{3}CT resulting in a small amount of reaction.

Other researchers[5,8] have concluded that intersystem crossing from higher Rh ^{1}LF excited states to the reactive lowest energy triplet state is very efficient ($\Phi_{isc} \simeq 1$) for $Rh(NH_3)_5L^{3+}$ complexes. Therefore, the inherent reactivity of the $^3T_1$ state of $Rh(NH_3)_5pyCN^{3+}$ is assumed equal to the Φ_{pyCN} value of 9.8×10^{-2} moles/ein., which was obtained upon irradiation of the monomer. The quantum yield for reactivity of the Rh(III) metal center (cleavage of the Rh-pyCN bond) upon irradiation of the Rh-pyCN-Ru binuclear complex was 1.06×10^{-3}moles/ein. Thus, the efficiency ($\Phi_{binuclear}/\Phi_{monomer}$) of the energy transfer or partitioning is 1.1%. These differences may reflect the efficiency of the energy transfer mechanism or differences in monomer and dimer lifetimes due to the perturbing influence of $Ru(NH_3)_5{}^{2+}$.

Term energy calculations, similar to those for $(NH_3)_5Rh(pyCN)Ru(NH_3)_5{}^{5+}$, were performed for $(NH_3)_5Rh(pyz)Ru(NH_3)_5{}^{5+}$. The ^{1}CT (Ru) manifold was estimated from the envelope of the band in the absorbance spectrum (~440 → 630 nm), and the upper and lower limits were set at 23 kK and 16 kK, respectively. The Rh(III) ^{3}LF energy is 19.7 kK[25], similar to that of the 4-cyanopyridine bridged binuclear complex.

The energy of the ^{3}LF (Ru) state for the Rh-pyz-Ru^{5+} complex should differ significantly from that of the Rh-pyCN-Ru^{5+} complex due to the change in ligand coordination. In Rh-pyCN-Ru^{5+}, the Ru(II) metal center is coordinated to the nitrile position, and values for $Ru(NH_3)_5acn^{2+}$

were used to determine the energy of the ^{3}LF (Ru) state (see equation (44)). In contrast, the Rh-pyz-Ru^{5+} complex has the Ru(II) coordinated to a pyridine-type position. Because of this, $Ru(NH_3)_6^{2+}$ values[45] were used to approximate the ^{3}LF (Ru) energy level (which is thus estimated to be near 17.4 kK). Figure 9 summarizes these calculations for $(NH_3)_5Rh(pyz)Ru(NH_3)_5^{5+}$.

The calculated energies of the ^{3}LF (Ru) and ^{1}CT levels are significantly lower in the Rh(pyz)Ru^{5+} complex than in the Rh(pyCN)Ru^{5+} complex. The energy of the ^{3}LF (Rh) level, however, was lowered only slightly by the change in bridging ligand. Thus, an energy partitioning reaction would be even more endergonic for the Rh(pyz)Ru^{5+} complex. In addition, a wavelength dependence for the quantum yield is exhibited. Irradiation of the complex at 436 nm resulted in a quantum yield for disappearance of starting material of 7.3 x 10^{-5} moles/ein., and irradiation at 546 nm gave a quantum yield of 2.8 x 10^{-6} moles/ein. These decreased quantum yields, when compared to the 4-cyanopyridine bridged complex, are consistent with the increased endergonic nature of the energy transfer or partitioning resulting from the lower ^{1}CT and ^{3}LF (Ru) levels relative to the ^{3}LF (Rh).

In addition, comparison of the quantum yields for the pyz- and 4-NCpy-bridged binuclear complexes indicates that the energy partitioning probably occurs from the ^{3}LF (Ru) level. The ^{1}CT energy manifold for Rh(pyz)Ru^{5+} is sufficiently high in energy such that if the energy transfer were to occur from that level, larger quantum yields would be expected.

Another mechanism which might explain the results obtained in the photolysis of the Rh(pyCN)Ru^{5+} binuclear complex is an electron transfer

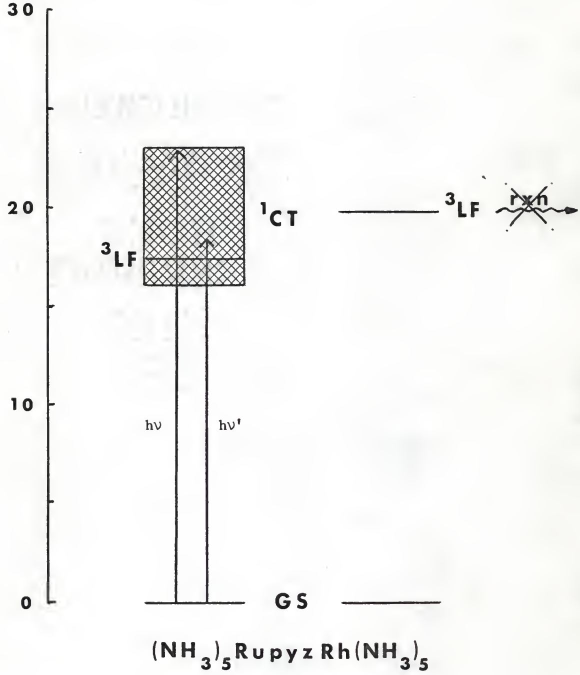

Figure 9. Energy level diagram for $(NH_3)_5Ru(pyz)Rh(NH_3)_5{}^{5+}$. hν corresponds to irradiation at 436 nm, hν' corresponds to irradiation at 546 nm.

from a CT excited state of the Ru(II) to the Rh(III). Loss of $RuNCpy^{2+}$ from the Rh metal center could result from a $(Rh^{II}\text{-pyCN-}Ru^{III})^*$ state (equation (45)), followed by outer-sphere back electron transfer to regenerate Rh(III) and Ru(II) fragments (equation (46)). A mechanism of

$$[(NH_3)_5Rh^{II}(pyCN)Ru^{III}(NH_3)_5]^* \rightarrow (NH_3)_5Ru^{III}NCpy + Rh^{II}(NH_3)_4 + NH_3 \quad (45)$$

$$(NH_3)_5Ru^{III}NCpy + Rh^{II}(NH_3)_4 + 2H_2O \rightarrow (NH_3)_5Ru^{II}NCpy + t\text{-}Rh^{III}(NH_3)_4(H_2O)_2 \quad (46)$$

this type has been observed upon photolysis of aqueous solutions of $Rh(NH_3)_5I^{2+}$[48]. Irradiation in the LMCT band of this complex initially resulted in the following reaction:

$$Rh(NH_3)_5I^{2+} + h\nu\ (LMCT) \xrightarrow{H+} Rh(NH_3)_4{}^{2+} + NH_4{}^+ + I\cdot \quad (47)$$

Recombination (redox) and aquation then occurred to form trans- $Rh(NH_3)_4$-OH_2I^{2+}.

Electrochemical data are not available to provide reduction potential values for the monomer components of $(NH_3)_5Rh(pyCN)Ru(NH_3)_5{}^{5+}$. Therefore, an estimate can not be made of the energy of irradiation required to result in an electron transfer. Reduction of Rh(III) to form Rh(II) is infrequent, as evidenced by polarographic studies which indicate a preference of Rh(III) to undergo a two electron reduction to form Rh(I)[49]. A one electron reduction case for Rh(III), in which LMCT irradiation of $Rh(NH_3)_5I^{2+}$ at 250 nm resulted in a substantial amount of electron transfer, makes it doubtful that irradiation of the 4-cyanopyridine bridged binuclear species at 436 nm would be sufficiently energetic to cause an electron transfer reaction from Ru(II) to Rh(III).

In addition, LMCT irradiation of $Rh(NH_3)_5I^{2+}$ results in recombination of the I· radical with the complex following reduction of the metal. Photolysis of the Rh-pyCN-Ru^{5+} complex, however, causes dissociation without recombination. This provides further evidence suggesting that an intramolecular electron transfer reaction is not occurring upon irradiation of the binuclear complex at 436 nm.

CONCLUSION

Photolysis of $(NH_3)_5Rh(pyz)Ru(NH_3)_5^{5+}$ leads to small quantum yields for photoaquation at either metal center. These results reflect the characteristic photochemistry of the Ru(II) monomer systems (i.e., "unreactive" for λ_{max} (MLCT) > 460-480 nm) and the fact that energy transfer to a Rh(III) ligand field excited state is endergonic and not likely to occur.

Based on the absorption spectra obtained during photolysis of $(NH_3)_5Rh(pyCN)Ru(NH_3)_5^{5+}$ and the calculations of approximate energy levels, irradiation of this complex leads to cleavage of the Rh(III)-pyridine nitrogen bond by either an energy transfer from the Ru(II) ^3CT state to the Rh(III) $^3T_1$ or an energy partitioning of ^3LF (Ru) → ^3LF (Rh) vs. ^3LF (Ru) → ^3CT. The product formed from the primary photochemical reaction, $Ru(NH_3)_5NCpy^{2+}$, then undergoes secondary photolysis to form $Ru(NH_3)_5H_2O^{2+}$.

Synthesis and photolysis of $[(NH_3)_5Rh(NCpy)Ru(NH_3)_5][ClO_4]_5$, the linkage isomer of the above complex, would provide corroboration of the concepts presented here. The $Ru(NH_3)_5pyCN^{2+}$ monomer has a MLCT absorption maximum near 500 nm[29]. Coordination to the Rh(III) metal center is expected to shift this band to an even longer wavelength. Thus, the calculated energies of the Ru(II) ^1CT and ^3CT bands would be significantly lower than those in the Rh-pyCN-Ru^{5+} complex, with the ^3LF (Ru) band remaining near 17.4 kK. The Rh(III) ^3LF energy level, however, would be lowered only a small amount by the decreased basicity of the $NCpyRu(NH_3)_5^{2+}$ ligand, as compared to the $pyCNRu(NH_3)_5^{2+}$ ligand. Therefore, an energy transfer from a Ru(II) MLCT level to the Rh(III) ^3LF is expected to be more endergonic in the Rh-NCpy-Ru^{5+} complex than in the Rh-pyCN-Ru^{5+} species, and would, thus, be even less likely to occur.

The behavior of $(NH_3)_5Rh(NCpy)Ru(NH_3)_5^{5+}$ would most likely parallel the reactivity of the pyrazine bridged dimer.

REFERENCES

1. V. Balzani and V. Carassiti, "Photochemistry of Coordination Compounds", Academic Press, Inc., New York, 1970.

2. R. B. Cundall and A. Gilbert, "Photochemistry", Appleton-Century-Crofts, New York, 1970.

3. a) B. N. Figgis, "Introduction to Ligand Fields", Wiley Interscience, New York, 1966, chapter 9.

   b) I. N. Levine, "Molecular Spectroscopy", Wiley Interscience, New York, 1975.

4. D. Sutton, "Electronic Spectra of Transition Metal Complexes", McGraw-Hill, London, 1968.

5. T. L. Kelly and J. F. Endicott, J. Phys. Chem., 76 (14), 1937, (1972).

6. C. Kutal and A. W. Adamson, Inorg. Chem., 12 (6), 1454, (1973).

7. M. M. Muir and W.-L. Huang, Inorg. Chem., 12 (8), 1831, (1973).

8. P. C. Ford, G. Malouf, J. D. Petersen and V. A. Durante, Adv. Chem. Ser., 150, 187, (1976).

9. J. D. Petersen, R. J. Watts, and P. C. Ford, J. Amer. Chem. Soc., 98, (11), 3188, (1976).

10. J. D. Petersen and P. C. Ford, J. Phys. Chem., 78 (12), 1144, (1977).

11. J. D. Petersen and F. P. Jakse, Inorg. Chem., 16 (11), 2845, (1977).

12. D. A. Chaisson, R. E. Hintze, D. H. Stuermer, J. D. Petersen, D. P. McDonald, and P. C. Ford, J. Amer. Chem. Soc., 94 (19), 6665, (1972).

13. G. Malouf and P. C. Ford, J. Amer. Chem. Soc., 96 (2), 601, (1974); ibid., 99, 7213, (1977).

14. W. L. Wells and J. F. Endicott, J. Phys. Chem., 75 (20), 3075, (1971).

15. R. Mason and D. M. P. Mingos, J. Organomet. Chem., 50, 53, (1973).

16. J. J. Lagowski, "Modern Inorganic Chemistry", Marcel Dekker, Inc., New York, 1973.

17. K. F. Purcell and J. C. Kotz, "Inorganic Chemistry", W. B. Saunders, Philadelphia, 1977.

18. H. Taube, Ber. Bunsen-Gesellschaft, 76 (10), 964, (1972).

19. C. Creutz and H. Taube, J. Amer. Chem. Soc., 95 (4), 1086, (1973).

20. J. K. Beattie, N. S. Hush, and P. R. Taylor, Inorg. Chem., 15 (4), 992, (1976).

21. M. S. Pereira and J. M. Malin, Inorg. Chem., 13 (2), 386, (1974).

22. V. A. Durante and P. C. Ford, J. Amer. Chem. Soc., 97 (23), 6898, (1975).

23. G. J. Leigh, Inorg. Chem., 17 (8), 2047, (1978).

24. S. N. Anderson and F. Basolo, Inorg. Syn., 7, 214, (1963).

25. J. D. Petersen, Doctoral Thesis, Univ..of Calif., Santa Barbara, (1975).

26. G. W. Bushnell, G. C. Lalor, and E. A. Moelwyn-Hughes, J. Chem. Soc. (A), 1966, 719.

27. R. E. Clarke, Master's Thesis. Univ. of Calif., Santa Barbara, (1969).

28. H. H. Schmidtke, Z. Phys. Chem., 45, 305, (1965).

29. R. E. Clarke and P. C. Ford, Inorg. Chem., 9 (3), 495, (1970).

30. J. L. Reed, H. D. Gafney, and F. Basolo, J. Amer. Chem. Soc., 96 (5), 1363, (1974).

31. R. B. Jordan, A. M. Sargeson, and H. Taube. Inorg. Chem., 5 (7), 1091, (1966).

32. J. G. Calvert and J. N. Pitts, Jr., "Photochemistry", John Wiley and Sons, New York, (1966), page 783.

33. E. E. Wegner and A. W. Adamson, J. Amer. Chem. Soc., 88, 394, (1966).

34. R. E. Clarke and P. C. Ford, Inorg. Chem., 9 (2), 227, (1970).

35. P. C. Ford, DeF. P. Rudd, R. Gaunder, and H. Taube, J. Amer. Chem. Soc., 90 (5), 1187, (1968).

36. J. E. Figard. J. V. Paukstelis, E. F. Byrne, and J. D. Petersen, J. Amer. Chem. Soc., 99 (26), 8417, (1977).

37. R. D. Foust, Jr. and P. C. Ford, Inorg. Chem., 11 (4), 899, (1972).

38. D. K. Lavallee, M. D. Baughman, and M. P. Phillips, J. Amer. Chem. Soc., 99 (3), 718, (1977).

39. J. Joussot-Dubien and J. Houdard, Tetrahedron Letters, 47, 4389, (1967).

40. H. Hartman and C. Buschbeck, Z. Phys. Chem., 11, 120, (1957).

41. M. Faraggi and A. Feder, Inorg. Chem., 12 (1), 236, (1973).

42. a) H. E. Toma and J. M. Malin, Inorg. Chem., 12 (5), 1039, (1973)
    b) H. D. Wohlers, "Photoaquation Reactions of Pentacyanocobaltate Complexes", A. C. S. Regional Meeting, Rolla, Missouri, Fall, 1978.

43. P. C. Ford, unpublished observations.

44. A. B. P. Lever, "Inorganic Electronic Spectroscopy", Elsevier Publishing Company, Amsterdan, The Netherlands, 1968.

45. P. C. Ford, Coord. Chem. Rev., 5, 75, (1970).

46. G. D. Hager and G. A. Crosby, J. Amer. Chem. Soc., 97 (24), 7031, (1975).

47. P. Grutsch and C. Kutal, J. Chem. Ed., 53 (7), 437, (1976).

48. T. L. Kelly and J. F. Endicott, J. Amer. Chem. Soc., 94 (6), 1797, (1972).

49. R. D. Gillard, B. T. Heaton, and D. H. Vaughn, J. Chem. Soc. (A), 1970, 3126.

Appendix A

Quantum Yield Calculation

Program for a Hewlett Packard 9810A Calculator

			Display		
Step	Key	Code	x	y	z
0	clear	20	0	0	0
1	stop	41	Δε	1	v
2	x	36	Δε	Δε•1	"
3	↓	25	Δε•1	v	"
4	÷	35	Δε•1	v/Δε•1	"
5	y→( )	40	"	"	"
6	0	00	"	"	"
7	0	00	"	"	"
8	0	00	"	"	"
9	stop	41	D.A.	I^{i}_{ℓ}	(Δε•1)
10	y→( )	40	"	"	"
11	0	00	"	"	"
12	0	00	"	"	"
13	1	01	"	"	"
14	x→( )	23	"	"	"
15	0	00	"	"	"
16	0	00	"	"	"
17	2	02	"	"	"
18	stop	41	real A^{o}_{irr}	A^{o}_{irr}	A^{o}_{mon}
19	x→( )	23	"	"	"
20	0	00	"	"	"
21	0	00	"	"	"
22	3	03	"	"	"
23	x→( )	23	"	"	"
24	0	00	"	"	"
25	0	00	"	"	"
26	4	04	"	"	"
27	y→( )	40	"	"	"
28	0	00	"	"	"
29	0	00	"	"	"
30	5	05	"	"	"
31	y→( )	40	"	"	"
32	0	00	"	"	"
33	0	00	"	"	"
34	6	06	"	"	"
35	↓	25	A^{o}_{irr}	A^{o}_{mon}	"
36	y→( )	40	"	"	"
37	0	00	"	"	"
38	0	00	"	"	"
39	7	07	"	"	"
40	y→( )	40	"	"	"
41	0	00	"	"	"
42	0	00	"	"	"
43	8	10	"	"	"

Step	Key	Code	Display		
			x	y	z
44	stop	41	A^t_{irr}	A^t_{mon}	t
45	pause	57	"	"	"
46	if flag	43	"	"	"
47	0	00	"	"	"
48	2	02	"	"	"
49	5	05	"	"	"
50	9	11	"	"	"
51	x→( )	23	"	"	"
52	0	00	"	"	"
53	0	00	"	"	"
54	9	11	"	"	"
55	y→( )	40	"	"	"
56	0	00	"	"	"
57	1	01	"	"	"
58	0	00	"	"	"
59	x←( )	67	"	"	"
60	−	34	"	"	"
61	0	00	"	"	"
62	0	00	"	"	"
63	6	06	"	"	"
64	y←( )	24	ΔA^{in}_{irr}	"	"
65	−	34	"	"	"
66	0	00	"	"	"
67	0	00	"		"
68	8	10	"	ΔA^{in}_{mon}	"
69	G	15	"	$\|\Delta A^{in}_{mon}\|$	"
70	y→( )	40	"	"	"
71	0	00	"	"	"
72	1	01	"	"	"
73	1	01	"	"	"
74	↑	22	t	ΔA^{in}_{irr}	$\|\Delta A^{in}_{mon}\|$
75	G	15	"	$\|\Delta A^{in}_{irr}\|$	"
76	y→( )	40	"	"	"
77	0	00	"	"	"
78	1	01	"	"	"
79	2	02	"	"	"
80	↑	27	"	t	$\|\Delta A^{in}_{irr}\|$
81	x←( )	67	"	"	"
82	−	34	"	"	"
83	a	13	Δt	"	"
84	x→( )	23	"	"	"
85	b	14	"	"	"
86	y→( )	40	"	"	"
87	a	13	"	"	"
88	x←( )	67	"	"	"
89	0	00	"	"	"
90	0	00	"	"	"
91	9	11	A^t_{irr}	"	"

			Display		
Step	Key	Code	x	y	z
92	x→( )	23	A^{t}_{irr}	t	$\lvert\Delta A^{in}_{irr}\rvert$
93	0	00	"	"	"
94	0	00	"	"	"
95	6	06	"	"	"
96	x←( )	67	"	"	"
97	–	34	"	"	"
98	0	00	"	"	"
99	0	00	"	"	"
100	5	05	ΔA^{ov}_{irr}	"	"
101	↑	27	"	ΔA^{ov}_{irr}	t
102	G	15	"	$\lvert\Delta A^{ov}_{irr}\rvert$	"
103	y→( )	40	"	"	"
104	0	00	"	"	"
105	1	01	"	"	"
106	3	03	"	"	"
107	x←( )	67	"	"	"
108	0	00	"	"	"
109	1	01	"	"	"
110	0	00	A^{t}_{mon}	"	"
111	x→( )	23	"	"	"
112	0	00	"	"	"
113	0	00	"	"	"
114	8	08	"	"	"
115	x←( )	67	"	"	"
116	–	34	"	"	"
117	0	00	"	"	"
118	0	00	"	"	"
119	7	07	ΔA^{ov}_{mon}	"	"
120	↑	27	"	ΔA^{ov}_{mon}	$\lvert\Delta A^{ov}_{irr}\rvert$
121	G	15	"	$\lvert\Delta A^{ov}_{mon}\rvert$	"
122	y→( )	40	"	"	"
123	0	00	"	"	"
124	1	01	"	"	"
125	4	04	"	"	"
126	x←( )	67	"	"	"
127	0	00	"	"	"
128	0	00	"	"	"
129	4	04	real A^{o}_{irr}	"	"
130	↑	27	"	real A^{o}_{irr}	$\lvert\Delta A^{ov}_{mon}\rvert$
131	x←( )	67	"	"	"
132	0	00	"	"	"
133	1	01	"	"	"
134	2	02	$\lvert\Delta A^{in}_{irr}\rvert$	"	"
135	–	34	"	real A^{t}_{irr}	"
136	↑	27	"	$\lvert\Delta A^{in}_{irr}\rvert$	real A^{t}_{irr}
137	2	02	2	"	"
138	÷	35	2	$\lvert\Delta A^{in}_{irr}\rvert/2$	"
139	y←( )	24	"	"	"

Step	Key	Code	Display		
			x	y	z
140	−	34	2	$\|\Delta A^{in}_{irr}\|/2$	real A^{t}_{irr}
141	0	00	"	"	"
142	0	00	"	"	"
143	4	04	"	$-A^{in}_{ave}$	"
144	↓	25	$-A^{in}_{ave}$	real A^{t}_{irr}	"
145	y→( )	40	"	"	"
146	0	00	"	"	"
147	0	00	"	"	"
148	4	04	"	"	"
149	↑	27	"	$-A^{in}_{ave}$	real A^{t}_{irr}
150	1	01	1	"	"
151	0	00	10	"	"
152	H	74	$10^{-A^{in}}$	"	"
153	chg sign	32	$-10^{-A^{in}}$	"	"
154	↑	27	"	$-10^{-A^{in}}$	$-A^{in}_{ave}$
155	1	01	1	"	"
156	+	33	1	$1-10^{-A^{in}}$	"
157	y←( )	24	"	"	"
158	x	36	"	"	"
159	0	00	"	"	"
160	0	00	"	"	"
161	1	01	"	$I^{i}_{o}(1-10^{-A^{in}})$	"
162	y←( )	24	"	"	"
163	x	36	"	"	"
164	b	14	"	quanta^{in}	"
165	y→( )	40	"	"	"
166	0	00	"	"	"
167	1	01	"	"	"
168	5	05	"	"	"
169	x←( )	67	"	"	"
170	1	01	"	"	"
171	3	03	$\|\Delta A^{ov}_{irr}\|$	"	"
172	↑	27	"	$\|\Delta A^{ov}_{irr}\|$	quanta^{in}
173	2	02	2	"	"
174	÷	35	"	$\|\Delta A^{ov}_{irr}\|/2$	"
175	y←( )	24	"	"	"
176	−	34	"	"	"
177	0	00	"	"	"
178	0	00	"	"	"
179	3	03	"	$-A^{ov}_{ave}$	"
180	1	01	1	"	"
181	0	00	10	"	"
182	H	74	$10^{-A^{ov}}$	"	"
183	chg sign	32	$-10^{-A^{ov}}$	"	"
184	↑	27	"	$-10^{-A^{ov}}$	$-A^{ov}_{ave}$
185	1	01	1	"	"
186	+	33	"	$1-10^{-A^{ov}}$	"
187	y←( )	24	"	"	"

Step	Key	Code	Display x	 y	 z
188	x	36	1	$1\text{-}10^{-A^{ov}}$	$-A^{ov}_{ave}$
189	0	00	"	"	"
190	0	00	"	"	"
191	1	01	"	$I^{i}_{o}(1\text{-}10^{-A^{ov}})$	"
192	y←( )	24	"	"	"
193	x	36	"	"	"
194	a	13	"	quanta^{ov}	"
195	x←( )	67	"	"	"
196	0	00	"	"	"
197	0	00	"	"	"
198	0	00	$v/\Delta\varepsilon\cdot 1$	"	"
199	x⇄y	30	quanta^{ov}	$v/\Delta\varepsilon\cdot 1$	"
200	÷	35	"	"	"
201	x←( )	67	"	"	"
202	0	00	"	"	"
203	1	01	"	"	"
204	4	04	$\|\Delta A^{ov}_{mon}\|$	"	"
205	x	36	"	Φ_{ov}/N	"
206	6	06	6	"	"
207	:	21	6.	"	"
208	0	00	6.0	"	"
209	2	02	6.02	"	"
210	3	03	6.023	"	"
211	ent. ex.	26	"	"	"
212	2	02	$6.023\text{x}10^{2}$	"	"
213	0	00	$6.023\text{x}10^{20}$	"	"
214	x	36	"	Φ_{ov}	"
215	↓	25	Φ_{ov}	$-A^{ov}_{ave}$	"
216	PR/SP	45	"	"	"
217	x←( )	67	"	"	"
218	0	00	"	"	"
219	1	01	"	"	"
220	4	04	$\|\Delta A^{ov}_{mon}\|$	"	"
221	x←( )	67	"	"	"
222	÷	35	"	"	"
223	0	00	"	"	"
224	0	00	"	"	"
225	2	02	% rxn	"	"
226	PR/SP	45	"	"	"
227	x←( )	67	"	"	"
228	0	00	"	"	"
229	0	00	"	"	"
230	0	00	$\Delta v/\Delta\varepsilon\cdot 1$	"	"
231	x←( )	67	"	"	"
232	x	36	"	"	"
233	0	00	"	"	"
234	1	01	"	"	"
235	1	01	n^{in}	"	"

			Display		
Step	Key	Code	x	y	z
236	x←( )	67	n^{in}	$-A^{ov}_{ave}$	$-A^{ov}_{ave}$
237	÷	35	"	"	"
238	0	00	"	"	"
239	1	01	"	"	"
240	5	05	Φ_{in}/N	"	"
241	↑	27	"	Φ_{in}/N	"
242	6	06	6	"	"
243	.	21	6.	"	"
244	0	00	6.0	"	"
245	2	02	6.02	"	"
246	3	03	6.023	"	"
247	ent. ex.	26	"	"	"
248	2	02	$6.023\text{x}10^{2}$	"	"
249	0	00	$6.023\text{x}10^{20}$	"	"
250	x	36	"	Φ_{in}	"
251	↓	25	Φ_{in}	$-A^{ov}_{ave}$	"
252	PR/SP	45	"	"	"
253	PR/SP	45	"	"	"
254	GO TO	44	"	"	"
255	0	00	"	"	"
256	0	00	"	"	"
257	4	04	"	"	"
258	4	04	"	"	"
259	PR/SP	45	"	"	"
260	PR/SP	45	"	"	"
261	PR/SP	45	"	"	"
262	PR/SP	45	"	"	"
263	PR/SP	45	"	"	"
264	PR/SP	45	"	"	"
265	PR/SP	45	"	"	"
266	PR/SP	45	"	"	"
267	PR/SP	45	"	"	"
268	END	46	"	"	"

Appendix B

Photolysis Data

Compound	Conditions	λ_{irr} (nm)	I_o^i (quanta/min.)	Φ_L (moles/ein.)	% reac.	Ref.
$[Rh(NH_3)_5pyz][ClO_4]_3$	nondeoxygenated, $1.9x10^{-3}$ $\underline{M}$, pH 2 $HClO_4$	313	$4.32x10^{17}$	-	-	15'-1-1
$[(NH_3)_5RhpyzRu(NH_3)_5][ClO_4]_5$	deoxygenated, $5.0x10^{-6}$ $\underline{M}$, pH 4 $HClO_4$	436	$3.34x10^{18}$	$6.60x10^{-5}$	3.7	34'-1-1
				$8.00x10^{-5}$	4.4	34'-1-2
		546	$2.11x10^{19}$	$2.76x10^{-6}$	3.6	35'-1-1
				$2.84x10^{-6}$	3.6	35'-1-2
$[Rh(NH_3)_5pyCN][ClO_4]_3$	nondeoxygenated, $2.7x10^{-3}$ $\underline{M}$, pH 2 $HClO_4$	313	$2.7x10^{17}$	$9.7x10^{-2}$	7.7	29-1-1
				$9.9x10^{-2}$	20.7	29-1-2
$[Ru(NH_3)_5NCpy][ClO_4]_2$	deoxygenated, ~$9.3x10^{-6}$ $\underline{M}$, pH 4 $HClO_4$	436	$1.14x10^{18}$	$4.85x10^{-2}$	92.2	58-1-1
				$2.50x10^{-2}$	88.5	58-1-2
			$1.15x10^{18}$	$1.96x10^{-2}$	41.5	59-1-1
				$2.05x10^{-2}$	33.1	59-1-2
			$1.24x10^{18}$	$1.40x10^{-2}$	32.1	61-1-1
				$2.27x10^{-2}$	85.7	61-1-2

Photolysis Data (cont.)

Compound	Conditions	λ_{irr} (nm)	I_o^i (quanta/min.)	Φ_L (moles/ein.)	% reac.	Ref.
$[(NH_3)_5RhpyCNRu(NH_3)_5][ClO_4]_5$	deoxygenated, ~$1.1x10^{-5}$ M, pH 4 $HClO_4$	436	$1.34x10^{18}$	$1.11x10^{-3}$	96.1	54-1-1
			$1.51x10^{18}$	$8.49x10^{-4}$	15.0	55-1-1
				$8.70x10^{-4}$	16.2	55-1-2
			$1.29x10^{18}$	$1.33x10^{-3}$	17.9	60-1-1
				$1.15x10^{-3}$	47.8	60-1-2
	$9.8x10^{-6}$ M	313	$9.4x10^{16}$	$1.18x10^{-2}$	18.5	56-1-2

THE PHOTOCHEMISTRY OF μ-PYRAZINEDECAAMMINERHODIUM(III)RUTHENIUM(II) PERCHLORATE AND μ-(4-CYANO-Ω*N*(Ru)-PYRIDINE-Ω*N*(Rh))-DECAAMMINERHODIUM(III)RUTHENIUM(II) PERCHLORATE

by

JANETTE ANN GELROTH

B.A., Bethany College, 1975

AN ABSTRACT OF A MASTER'S THESIS

submitted in partial fulfillment of the

requirements for the degree

MASTER OF SCIENCE

Department of Chemistry

KANSAS STATE UNIVERSITY
Manhattan, Kansas

1979

The visible light photolysis of μ-pyrazinedecaamminerhodium(III)-ruthenium(II) perchlorate, $[(NH_3)_5Rh(pyz)Ru(NH_3)_5][ClO_4]_5$, and μ-(4-cyano-$\Omega N$(Ru)-pyridine-$\Omega N$(Rh))decaamminerhodium(III)ruthenium(II) perchlorate, $[(NH_3)_5Rh(pyCN)Ru(NH_3)_5][ClO_4]_5$, are reported in this study. Irradiation of the former binuclear complex did not result in measurable photosubstitution reactions. Irradiation of the latter complex in the spectral region corresponding to a Ru(II) → 4-cyanopyridine charge transfer transition resulted in cleavage of the Rh-pyCN bond, a reaction characteristic of a ligand field excited state for a rhodium monomer. These data are discussed in terms of a mechanism which relies on intramolecular energy transfer between the metal centers in the binuclear complex. Comparisons will be made in assessing the photochemical reactions of the binuclear complexes in terms of the mononuclear fragments.